AD-A191 879 INTERACTION OF ULTRASONIC WAVES WITH COMPOSITE PLATES (U) CINCINNATI UNIV OH DEPT OF AEROSPACE ENGINEERING AND ENGINEERING MECHANICS A H NAYFEH 15 DEC 87 1/1

UNCLASSIFIED AFOSR-TR-88-0259 AFOSR-86-0052 F/G 11/4 NL

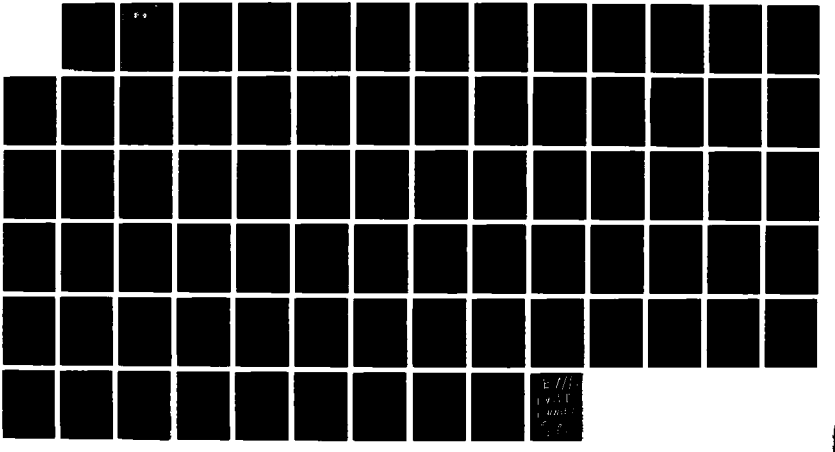

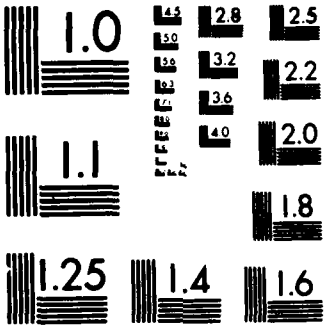

DTIC FILE COPY (2)

AD-A191 879

DTIC ELECTED S MAR 09 1988 D

REPORT DOCUMENTATION PAGE

1a. REPORT SECURITY CLASSIFICATION: UNCLASSIFIED	1b. RESTRICTIVE MARKINGS
2a. SECURITY CLASSIFICATION AUTHORITY	3. DISTRIBUTION/AVAILABILITY OF REPORT: UNLIMITED
2b. DECLASSIFICATION/DOWNGRADING SCHEDULE	
4. PERFORMING ORGANIZATION REPORT NUMBER(S)	5. MONITORING ORGANIZATION REPORT NUMBER(S): AFOSR-TR- 88-0259
6a. NAME OF PERFORMING ORGANIZATION: University of Cincinnati; 6b. OFFICE SYMBOL (If applicable)	7a. NAME OF MONITORING ORGANIZATION: AFOSR/NE
6c. ADDRESS (City, State and ZIP Code): DEPT OF AEROSPACE ENGINEERING & MECHANICS, Cincinnati, OH 45221	7b. ADDRESS (City, State and ZIP Code): BLDG 410, Bolling AFB, DC 20332-6448
8a. NAME OF FUNDING/SPONSORING ORGANIZATION: SAME AS 7a; 8b. OFFICE SYMBOL (If applicable)	9. PROCUREMENT INSTRUMENT IDENTIFICATION NUMBER: AFOSR-86-0052
8c. ADDRESS (City, State and ZIP Code): SAME AS 7b	10. SOURCE OF FUNDING NOS.

PROGRAM ELEMENT NO.	PROJECT NO.	TASK NO.	WORK UNIT NO.
61102F	2306	A3	

11. TITLE (Include Security Classification): Interaction of Ultrasonic Waves With Composite Plates

12. PERSONAL AUTHOR(S): NAYFEH

13a. TYPE OF REPORT	13b. TIME COVERED	14. DATE OF REPORT (Yr., Mo., Day)	15. PAGE COUNT
ANNUAL REPORT	FROM 15/12/86 TO 15/12/87		

16. SUPPLEMENTARY NOTATION

17. COSATI CODES		
FIELD	GROUP	SUB. GR.

18. SUBJECT TERMS (Continue on reverse if necessary and identify by block number)

19. ABSTRACT (Continue on reverse if necessary and identify by block number)

During the secon year of our reporting period we continued our close cooperation with the NDE Branch on the Materials Lab at Wright-Patterson Air Force Base. For our part, we continued developing analytical and computational methods on the modeling of the mechanical behavior of fibrous composities for applications in the NDE field. Specifically, we extended our theoretical models which were developed to describe the behavior of single unidirectional fiber reinforced plates, to more general plates. These included single and multilayered plates. For the single laminated plate the solutions are extended for arbitrary azimuthal angles and hence resulted in three dimensional analysis.

20. DISTRIBUTION/AVAILABILITY OF ABSTRACT	21. ABSTRACT SECURITY CLASSIFICATION
UNCLASSIFIED/UNLIMITED ☐ SAME AS RPT. ☐ DTIC USERS ☐	UNCLASSIFIED

22a. NAME OF RESPONSIBLE INDIVIDUAL	22b TELEPHONE NUMBER (Include Area Code)	22c. OFFICE SYMBOL
WEINSTOCK	(202) 767-4933	AFOSR/NE

DD FORM 1473, 83 APR EDITION OF 1 JAN 73 IS OBSOLETE

SECURITY CLASSIFICATION OF THIS PAGE

ANNUAL TECHNICAL REPORT

Grant: AFOSR-86-0052

Period December 15, 1986 - December 15, 1987

Interaction of Ultrasonic Waves With Composite Plates

Adnan H. Nayfeh

Department of Aerospace Engineering and Engineering Mechanics
University of Cincinnati
Cincinnati, OH 45221

INTERACTION OF ULTRASONIC WAVES WITH COMPOSITE PLATES

ADNAN H. NAYFEH

Department of aerospace Engineering and Engineering Mechanics,

University of Cincinnati, Cincinnati, Ohio 45221

ABSTRACT

During the second year of our reporting period we continued our close cooperation with the NDE Branch of the Materials Lab at Wright-Patterson Air Force Base. For our part, we continued developing analytical and computational methods on the modeling of the mechanical behavior of fibrous composites for applications in the NDE field. Specifically, we extended our theoretical models which were developed to describe the behavior of single unidirectional fiber-reinforced plates, to more general plates. These included single and multilayered plates. For the single laminate plate the solutions are extended for arbitrary azimuthal angles and hence resulted in three-dimensional analysis. However, for the general multilayered plate case, treatment so far has been restricted to the case where the individual lamina component of the plate is isotropic. Reflection and transmission coefficients are derived, from which characteristic behavior is identified. This was verified experimentally by the scientific group at Wright Patterson. These combined efforts contributed to an advancement of the state-of-the-art of the NDE methods. As described below our recent efforts resulted in several presentations and publications in the open literature.

I. Fluid-Coupled Wave Propagation in Orthotropic Plates With Application to Fibrous Composites

I.1 Introduction

In recent years considerable efforts have been expended upon the modeling, testing and analysis of fibrous composites. This is due in part to their popularity in applications requiring high stiffness to weight ratios and also to their intrinsic interest as challenging mechanical systems. However, the morphology of fiber-reinforced composites, as compared with that of homogeneous isotropic media, can seriously complicate their mechanical response. For example, these materials differ from isotropic homogeneous materials in that they are anisotropic and dispersive. The degrees of anisotropy and dispersivity depend upon the specific material under consideration and also upon the specific application, however.

Since most fibrous structural components are subjected to cyclic or impulsive loads which can lead to degradation in load-carrying capability, initial inspection and continued monitoring of these materials for detection and sizing of strength-degrading flaws is necessary in order to insure structural reliability. Ultrasonic nondestructive evaluation is one useful means to provide information related to structural integrity of composites. To assist in the exploitation of this technique for inspecting composites, a full understanding of the propagation of elastic waves in fibrous composites is highly desirable.

Compared with the voluminous literature on the propagation of elastic waves in isotropic media, a limited amount of work exists on anisotropic materials. This is particularly true for the classes of guided waves such as surface, Love, Lamb, and Stonely waves. Investigation of the propagation of bulk waves in anisotropic materials is relatively well established (see,

for example, Musgrave [1], Synge [2] and Fedorov [3]). Comparatively speaking, few quantitative results have been reported on solutions of guided waves in anisotropic media.

Several authors [4-14] have discussed the reflection and refraction problems from interfaces of anisotropic media in varying degrees of detail. Stonely, in 1955, studied Rayleigh surface wave propagation on an anisotropic half-space having cubic crystal symmetry [15]. Since then several other authors [16-22] have considered and reported on similar problems. Theoretical analyses have been undertaken for free Lamb waves in plates of orthotropic [23-24] , transversely isotropic [25-27] and cubic [28-29] materials.

Because fiber-reinforced composites are often employed in plate-like structures and ultrasonic testing is conveniently performed in immersion, we recently investigated both theoretically and experimentally the behavior of guided elastic waves in fluid-coupled plates of unidirectional fibrous composites [30,31]. For consistency we refer, in our work, to the fluid-coupled modes as plate modes. These exitations may be contrasted with Lamb modes for a plate in vacuum, like that studied in [32,33]. In [30,31] results were presented for cases where the plate wave vector is along the direction of symmetry, i.e., the fiber axis.

We present a unified analytical treatment of ultrasonic waves with generally orthotropic elastic plates. The plates are assumed to be immersed in a fluid and subjected to incident acoustic waves at arbitrary angles from the normal as well as at arbitrary azimuthal angles. Reflection and transmission coefficients are derived from which characteristic features are identified. Highly complex reflection behavior, expressed as phase velocity-frequency dispersion, is observed in the model prediction. Our

analytical modeling has been compared with the extensive experimental data collected by Chimenti of the Air Force Material Laboratory in ultrasonic reflection measurements on a plate of T300/Ciba-Geigy 914 composite, selected as a model system to test the theory. Comparisons between theoty and experiment show excellent agreement is seen in curves at several azimuthal angles between $0^{\circ}$and 90°, despite complicated features in the results.

A key condition which is found to facilitate our subsequent analysis is the fact that the wave vectors of the incident and refracted waves must all lie in the same plane. This result is a consequence of satisfying continuity conditions at the fluid-solid interface (see [10] for justification). We will therefore conduct our analysis in a coordinate system formed by incident and interfacial planes rather than by material symmetry axes. This condition leads to a simplification in our algebraic analysis and computations.

I.2 Theory

Consider an infinite orthotropic plate having the thickness d and immersed in fluid such that its symmetry axes are oriented originally along the cartesian coordinate system $x_i' = (x_1', x_2', x_3')$. The plane x_1'-x_2' is chosen to coincide with the upper surface of the plate, and the x_3' coordinate is normal to it, as illustrated in Fig. 1. With respect to this primed coordinate system, the elastic field equations of the plate are given by the momentum equations

$$\frac{\partial \sigma_{ij}}{\partial x_j'} = \rho \frac{\partial^2 u_i'}{\partial t^2} \qquad (1)$$

and, from the general constitutive relations for anisotropic media,

$$\sigma'_{ij} = c'_{ijk\ell} \; e'_{k\ell} \tag{2}$$

by the specialized expanded matrix form to orthotropic media

$$\begin{vmatrix} \sigma'_{11} \\ \sigma'_{22} \\ \sigma'_{33} \\ \sigma'_{23} \\ \sigma'_{13} \\ \sigma'_{12} \end{vmatrix} = \begin{vmatrix} C'_{11} & C'_{12} & C'_{13} & 0 & 0 & 0 \\ C'_{12} & C'_{22} & C'_{23} & 0 & 0 & 0 \\ C'_{13} & C'_{23} & C'_{33} & 0 & 0 & 0 \\ 0 & 0 & 0 & C'_{44} & 0 & 0 \\ 0 & 0 & 0 & 0 & C'_{55} & 0 \\ 0 & 0 & 0 & 0 & 0 & C'_{66} \end{vmatrix} \begin{vmatrix} e'_{11} \\ e'_{22} \\ e'_{33} \\ \gamma'_{23} \\ \gamma'_{13} \\ \gamma'_{12} \end{vmatrix} \tag{3}$$

where we used the contracting subscript notations 1→11, 2→22, 3→33, 4→23, 5→13 and 6→12 to relate $c'_{ijk\ell}$ to C'_{pq} ($i,j,k,\ell = 1,2,3$ and $p,q = 1,2....6$). Thus, C'_{55} stands for C_{1313}, for example. Here σ_{ij}, e_{ij} and u'_i are the components of stress, strain and displacement, respectively, and ρ is the material density. In Eq. (3), $\gamma_{ij} = 2e_{ij}$ (with $i \neq j$) defines the engineering shear strain components.

Since $c'_{ijk\ell}$ is a fourth order tensor, then for any orthogonal transformation of the primed to the non-primed coordinates, i.e., x'_i to x_i, it transforms according to

$$c_{mnop} = \beta_{mi} \; \beta_{nj} \; \beta_{ok} \; \beta_{p\ell} \; c'_{ijk\ell} \tag{4}$$

where β_{ij} is the cosine of the angle between x_i' and x_j, respectively. For a rotation of angle ϕ in the x_1' -x_2' plane, the transformation tensor β_{ij} reduces to

$$\begin{vmatrix} \cos\phi & \sin\phi & 0 \\ -\sin\phi & \cos\phi & 0 \\ 0 & 0 & 1 \end{vmatrix} \tag{5}$$

which, if applied to Eq. (2) through the relation of Eq. (3) yields

$$\begin{vmatrix} \sigma_{11} \\ \sigma_{22} \\ \sigma_{33} \\ \sigma_{23} \\ \sigma_{13} \\ \sigma_{12} \end{vmatrix} = \begin{vmatrix} C_{11} & C_{12} & C_{13} & 0 & 0 & C_{16} \\ C_{12} & C_{22} & C_{23} & 0 & 0 & C_{26} \\ C_{13} & C_{23} & C_{33} & 0 & 0 & C_{36} \\ 0 & 0 & 0 & C_{44} & C_{45} & 0 \\ 0 & 0 & 0 & C_{45} & C_{55} & 0 \\ C_{16} & C_{26} & C_{36} & 0 & 0 & C_{66} \end{vmatrix} \begin{vmatrix} e_{11} \\ e_{22} \\ e_{33} \\ \gamma_{23} \\ \gamma_{13} \\ \gamma_{12} \end{vmatrix} \tag{6}$$

where the transformation relations between the C_{pq} and C'_{pq} entries are listed in Appendix A. Notice that, no matter what rotational angle ϕ is used, the zero entries in Eq. (6) will remain zero. In fact, the matrix of Eq. (6), although particularized to orthotropic media, resembles that of monoclinic media (i.e. media which has $x_3 = 0$ as a plane of symmetry). In terms of the rotated coordinate system x_k, we write the momentum equations as

$$\frac{\partial \sigma_{ij}}{\partial x_j} = \rho \frac{\partial^2 u_i}{\partial t^2} \tag{7}$$

Substituting from Eq. (6) into Eq. (7) results in a system of three coupled equations for the displacements u_1, u_2 and u_3. If we now identify

the plane of incidence to be the x_1-x_3, as in Fig. 1, a formal solution for the displacements u_i can be written as

$$(u_1,u_2,u_3) = (1,V,W)Ue^{i\xi(x_1 + \alpha x_3 - ct)} , \qquad (8)$$

where ξ is the wave number, c is the phase velocity ($=\omega/\xi$), ω is the circular frequency, α is still an unknown parameter, and V,W are ratios of the displacement amplitudes of u_2 and u_3 to u_1, respectively. Combinations of Eqs. (8), (7) and (6) yield the matrix relation

$$\begin{vmatrix} C_{11} - \rho c^2 + C_{55}\alpha^2 & C_{16} + C_{45}\alpha^2 & (C_{13} + C_{55})\alpha \\ C_{16} + C_{45}\alpha^2 & C_{66} - \rho c^2 + C_{44}\alpha^2 & (C_{36} + C_{45})\alpha \\ (C_{13} + C_{55})\alpha & (C_{36} + C_{45})\alpha & C_{55} - \rho c^2 + C_{33}\alpha^2 \end{vmatrix} \begin{vmatrix} 1 \\ V \\ W \end{vmatrix} = 0 \quad (9)$$

Nontrivial solutions for V and W demand the vanishing of the determinant in equation (9) and yield an algebraic equation relating α to c. This equation is reduced (see Appendix B) to a sixth-degree polynomial equation in α, namely

$$\alpha^6 + A_1\alpha^4 + A_2\alpha^2 + A_3 = 0 \qquad (10)$$

Equation (10) admits three solutions for α^2 which we label as α_1^2, α_3^2 and α_5^2. These lead to six solutions for α which we further label as

$$\alpha_2 = -\alpha_1, \ \alpha_4 = -\alpha_3 \text{ and } \alpha_6 = -\alpha_5 \qquad (11)$$

Using superposition, together with the relation (9), we can relate the displacement ratios V_q and W_q for each α_q as

$$V_q = \frac{F_{23}(F_{11} + C_{55}\alpha_q^2) - (F_{12} + C_{45}\alpha_q^2)F_{13}}{F_{13}(F_{22} + C_{44}\alpha_q^2) - (F_{12} + C_{45}\alpha_q^2)F_{23}} \tag{12}$$

$$W_q = \alpha_q \frac{F_{23}(F_{11} + C_{55}\alpha_q^2) - (F_{12} + C_{45}\alpha^2)F_{13}}{(F_{12} + C_{45}\alpha_q^2)(F_{33} + C_{33}\alpha_q^2) - F_{13}F_{23}\alpha_q^2}, \quad q = 1,2...6 \tag{13}$$

where F_{st} ,s,t= 1,2,3 are defined in Appendix B. Combining Eqs. (12) and (13) with the stress-strain relations Eq. (6), we rewrite the formal solutions for the displacements and stresses as

$$(u_1,u_2,u_3) = \sum_{q=1}^{6} (1, V_q, W_q)U_q \, e^{i\xi(x_1+\alpha_q x_3-ct)} \tag{14}$$

$$(\sigma_{33},\sigma_{13},\sigma_{23}) = \sum_{q=1}^{6} (D_{1q},D_{2q},D_{3q})U_q e^{i\xi(x_1+\alpha_q x_3-ct)} \tag{15}$$

where

$$D_{1q} = C_{13} + C_{36} V_q + C_{33} \alpha_q W_q \tag{16a}$$

$$D_{2q} = C_{55}(\alpha_q + W_q) + C_{45} \alpha_q V_q \tag{16b}$$

and

$$D_{3q} = C_{45}(\alpha_q + W_q) + C_{44} \alpha_q V_q \quad , q = 1,2,...,6 \tag{16c}$$

With reference to Eq. (11) and by inspection of Eqs. (12) - (16c) one deduces the relations

$$V_2 = V_1, \; V_4 = V_3, \; V_6 = V_5 \tag{17a}$$

$$W_2 = -W_1, \; W_4 = -W_3, \; W_6 = -W_5 \tag{17b}$$

$$D_{12} = D_{11}, \; D_{14} = D_{13}, \; D_{16} = D_{15} \tag{18a}$$

$$D_{22} = -D_{21}, \; D_{24} = -D_{23}, \; D_{26} = -D_{25} \tag{18b}$$

$$D_{32} = -D_{31}, \; D_{34} = -D_{33}, \; D_{36} = -D_{35} \tag{18c}$$

I.3 Derivayion of the Reflection and Transmission Coefficients

To determine the reflection and transmission coefficients for plane waves incident from the fluid onto the plate surface at an arbitrary angle θ we need to obtain general solutions for the upper and lower fluids similar to those of Eqs. (14) and (15). Recognizing that the fluid does not support shear deformation, its field equations reduce to

$$\frac{\partial \sigma_{ij}^{(f)}}{\partial x_j} = \rho_f \frac{\partial u_i^{(f)}}{\partial t^2} \tag{19}$$

$$\sigma_{ij}^{(f)} = \lambda_f \frac{\partial u_k^{(f)}}{\partial x_k} \delta_{ij}, \qquad i,j = 1,2,3, \tag{20}$$

where both equations hold only for i=j; ρ_f and λ_f are the fluid density and Lame' constant. If the wave is assumed to be incident and hence reflected in the upper fluid and transmitted into the lower fluid, then using similar analysis to that of the plate yields, for the upper fluid,

$$(u_1,u_2,u_3,\ \sigma_{33})^{(u)} = \sum_{k=1}^{2} (1,0,W_k^{(u)}, i\xi\rho_f c^2)U_k^{(u)} e^{i\xi[x_1+(-1)^{k+1}\alpha_f x_3 - ct]} \tag{21}$$

and for the lower fluid

$$(u_1,u_2,u_3,\ \sigma_{33})^{(\ell)} = (1,0,\alpha_f, i\xi\rho_f c^2)U^{(\ell)} e^{i\xi[x + \alpha_f(x_3-d)-ct]}, \tag{22}$$

where

$$W_1^{(u)} = \alpha_f, \quad W_2^{(u)} = -\alpha_f \tag{23a}$$

$$\alpha_f = \left(\frac{c^2}{c_f^2} - 1\right)^{\frac{1}{2}}, \quad c_f = \left(\frac{\lambda_f}{\rho_f}\right)^{\frac{1}{2}} \tag{23b}$$

Notice the vanishing of shear component u_2 in both the upper and lower fluids.

By invoking the continuity of the normal displacements and stresses at $z = 0$ and $z = d$ and setting the solid shear stresses σ_{13} and σ_{23} equal to zero at $z = 0$ and $z = d$ we obtain, for a given incident amplitude U_1^u, a system of eight linear simultaneous equations for the amplitudes $U_2^{(u)}$, U^{ℓ}, U_1, U_2, U_3, U_4, U_5 and U_6 is obtained. Solving these equations with the help of the relations (17) and (18) and applying rather lengthy algebraic reductions and manipulations, we derive the following expressions for the reflection and the transmission coefficients

$$R = \frac{U_2^{(u)}}{U_1^{(u)}} = \frac{AS-Y^2}{(S+iY)(A-iY)} \tag{24}$$

$$T = \frac{U^{(\ell)}}{U_1^{(u)}} = \frac{iY(S+A)}{(S+iY)(A-iY)} \tag{25}$$

where

$$S = D_{11}G_1\cot(\gamma\alpha_1) - D_{13}G_3\cot(\gamma\alpha_3) + D_{15}G_5\cot(\gamma\alpha_5) \tag{26a}$$

$$A = D_{11}G_1\tan(\gamma\alpha_1) - D_{13}G_3\tan(\gamma\alpha_3) + D_{15}G_5\tan(\gamma\alpha_5) \tag{26b}$$

$$Y = \frac{\rho_f c^2}{\alpha_f}\ (W_1G_1 - W_3G_3 + W_5G_5) \tag{26c}$$

with

$$G_1 = D_{23}D_{35} - D_{33}D_{25} \tag{27a}$$

$$G_3 = D_{21}D_{35} - D_{31}D_{25} \tag{27b}$$

$$G_5 = D_{21}D_{33} - D_{31}D_{23} \tag{27c}$$

$$\gamma = \xi d/2 = \omega d/2c. \tag{27d}$$

Except for the more complicated definitions of the functions S,A and Y, the expressions R and T resemble those reported in our earlier paper [31], and our notation was chosen for consistency with this previous calculation.

I.4 Results and Discussion

In comparisons between the results of many measurements at several azimuthal angles and the model calculation, we have concentrated our attention, as in previous investigations [30,31], on the reflection coefficient. Since the basis of the experimental data is an amplitude signal in the reflected field of the incident beam, we calculate the plane-wave reflection coefficient for the plate and investigate it for the same type of behavior as we observe in the measurements. In addition to direct comparisons of amplitude spectra, we have also expressed our results as dispersion-like curves, where the results correspond to functions conditioned by the reflection coefficient. Both of these aspects of our studies are presented below.

A finite ultrasonic beam is composed of a range of plane wave components which define its angular spread,

$$\beta(x) = \int \hat{\beta}(\xi)\exp(-2\pi i\xi x)d\xi \qquad (29)$$

where $\beta(x)$ is the one-dimensional real space incident beam profile, x is a coordinate perpendicular to the beam direction, and the caret denotes Fourier transform. When such a finite beam interacts with a plate, each Fourier component of the incident field will contribute to the reflected field, weighted by the appropriate value of the reflection coefficient for that ξ. The resulting expression for the reflected field is given by

$$A(Fd,x_1) = \int\hat{\beta}(\xi)R(\xi,Fd)\exp[-2\pi i\xi(x_1-\alpha_f x_3)]d\xi \qquad (30)$$

where $R(\xi,Fd)$ is the reflection coefficient from Eq. (24) for the composite plate. The expression of Eq. (30) evaluated over frequency is an approximation to the experimental spectrum of the plate, if the beam profile $\beta(x)$ is chosen to represent the incident beam. We have performed such calculations for a variety of experimental conditions. Some typical comparisons are contained in Figs. 3(a)-(d).

Figure 3(a) shows the measured and predicted spectra from 1 to 8 MHz for an incident angle $\theta = 12°$ and azimuthal angle $\phi = 30°$. The two curves have been vertically scaled, but in no other way adjusted. The solid curve is the expression of Eq. (30), and the dashed curve is the experimental data deconvolved to remove transducer response. Positions of the deep minima in the two curves are nearly coincident, as we have observed for propagation in the fiber direction [31]. We conjecture that the additional shallower sharp dips, some of which do not appear in the data, arise from the coupling between vertical and horizontal shear displacements, referred to in the Theory section, which occurs for propagation in a general azimuthal direction. At $\theta = 28°$ and $\phi = 15°$ in Fig. 3(b), similar results are found, where the general trend of the data is well reproduced by the model calculation. In particular, the two shallower minima between 2 and 4 MHz are given fairly accurately by the prediction. This structure disappears for $\phi = 0°$, leaving only the deep minima at 1.9, 4.3 MHz, and beyond. Holding the incident angle constant and incrementing ϕ to 30°, the structure of the curve has evolved in Fig. 3(c) with the two minima near 3 MHz approaching each other more closely and deepening considerably. These features are also seen in the model calculations. In the final frame, Fig. 3(d), results are given for $\theta = 24°$ and $\phi = 90°$. This case corresponds to symmetry axis propagation, and therefore the complex structure of the

previous examples is largely absent. The positions of the minima are well modeled by the theory, whereas the minor differences in the lineshape details may be attributed to wavefront distortion and sound absorption, neither of which is considered in the model.

Taking the results of many dozens of experimental spectra such as those shown in Fig. 3 and recording the minima as a function of the incident angle (expressed through Snell's law as a phase velocity), yields a dispersion-like plot of the ultrasonic reflection behavior. In previous work [31,36] we demonstrated that the hypothesis of Cremer [37] concerning the coincidence of reflection minima with the excitation of Lamb wave modes is not well satisfied in all regions of plate wave dispersion in graphite-epoxy composites. Therefore, although we present these data in the manner of a velocity dispersion curve, it must be stressed that it is the reflection properties which are being reported.

Figure 4(a) shows data acquired in the current study at an azimuthal angle $\phi = 0°$ plotted together with the results of the analytical prediction derived by examining the behavior of the reflection coefficient, Eq. (24). To obtain the theory curves rapid phase variations in the reflection coefficient, generally indicative of total transmission, have been recorded as a function of Fd for many values of phase velocity. These calculations are presented as small filled circles which coalesce into solid curves over most of the plot. In some cases to be discussed a dashed line has been added as a guide to the eye. In Fig. 4(a) the data, plotted as discrete crosses, are in excellent agreement with the prediction of our new, more general model. All features of the data from $\theta = 12°$ to $\theta = 40°$ are well explained in the model. Propagation in the other material symmetry direction $\phi = 90°$ is shown in Figure 4(b). Here the results reflect the

substantial effective softening of the composite as the fiber axis is rotated out of the plane of incidence. Therefore, we observe a marked reduction in the phase velocities at which certain features occur. The vertical intercept of the curve, which is similar to the S_0 mode, is seen to be near c_p = 2.2 km/sec. Likewise, the point of diminishing slope of some of the higher order curves is much lower here than for $\phi = 0°$ as in Fig. 4(a). In fact, the behavior referred to is not even visible in Fig. 4(a) because it occurs above c_p = 9.8 km/sec.

For a transversely isotropic material, setting $\phi = 90°$ implies that elastic behavior in the plane of the incidence ($x_2' - x_3'$ plane) will be isotropic. An important experimental finding of the present study is the suggestion that transverse isotropy is not an appropriate symmetry class for the eight-ply Thornel/Ciba-Geigy *composite* sample we studied. Our result on the inequality of C_{22}' and C_{33}' stands in contrast to previous investigations, both mechanical [38] and ultrasonic [39], on thick-section T300 - 5208 unidirectional composite. In these earlier studies the ratio C_{22}'/C_{33}' was measured to be within 2% of unity. Because of the method of fabrication of these materials in which compressive stresses are exerted on the surfaces of the curing composite, fibers might tend to be distributed nonuniformly in the plate. That is, the number of fibers per unit length in the x_3' direction could be higher than the same quantity in the x_2' direction (refer to Eqs. (1)-(3)). Our experimental data for $\phi = 90°$ are consistent with the above interpretation and draw us to the conclusion that orthotropy is the correct symmetry class for thin sections of this material. Since the elastic constant denoted C_{22}' in Eq. (3) is difficult to measure

independently, we have inferred this quantity from our reflection data and the model calculation. The results of this evaluation yield a ratio of C'_{22} to C'_{33} of 0.72. Once this adjustment in C'_{22} is made, all subsequent comparisons at intermediate values of ϕ are carried out, using this same constant. Here we note that C'_{22} does not influence the propagation behavior along $\phi = 0°$, and hence this issue was not encountered in our previous work [31]. A set of slowness curves with the elastic constants of [35] for orthotropic graphite epoxy at $\phi = 90°$ is shown in Fig. 5. This representation illustrates the degree of anisotropy in the $x'_2 - x'_3$ plane. It may be noted that while the quasilongitudinal and slow quasitransverse wavespeeds vary with propagation direction in this plane, the fast quasitransverse wave is still isotropic. Of course, if the composite were transversely isotropic, all three slowness curves would be circles with the two transverse waves coincident.

If we now depart from the principal axis directions, the reflection behavior becomes substantially more complicated, as can be seen in Fig. 6(a) for $\phi = 30°$. The simple structure of Fig. 4(a) is replaced by curves which split apart, rejoin, and cross over each other. Throughout the range of the measurements, relatively good agreement with the theory is apparent. Although interpretation of these results is delicate, we may note a few arguably consistent trends. As the fiber direction is rotated out of the plane of incidence, the effective material constants begin to soften, causing the phase velocity intercept of the S_0-like curve to decrease, as in Fig. 4(b). In Fig. 6(a) that velocity is about 8.5 km/sec, whereas the value is 9.8 km/sec for propagation along the fibers. Moreover, an additional set of curves seems to have nucleated, in agreement with our

calculations and data starting as low as $\phi = 15°$. These general features will be seen to persist in the results for higher values of ϕ as well.

Comparison of measurement and theory for $\phi = 45°$ is contained in Fig. 6(b). As expected, the intercept velocity has decreased to about 7 km/sec, and behavior of even higher complexity has appeared above this value. The series continues with $\phi = 60°$ in Fig. 6(c), where the overall pattern established earlier is evident here also. Finally, in Fig. 6(d) for $\phi = 75°$ we have the last of the comparisons. The intercept velocity here is near 3.4 km/sec, nearly a factor of 3 below its $\phi = 0°$ value. These curves contain an almost unbelievably rich variety of reflection phenomena, considering the relatively simple form of the $\phi = 0°$ curves in Fig. 4(a). As we have stated earlier, it is our conjecture that these additional features arise from the coupling of the vertical and horizontal quasitransverse waves, which are independent for propagation along principal axes. We note in closing this section that in all these comparisons, but especially Figs. 6(c) and 6(d), agreement between measurements and theory is not simply a matter of general trends. Excellent detailed agreement is seen over most of these plots, in spite of the richly complex behavior observed for a general azimuthal angle. This observation lends confidence in the validity of the theoretical approach.

II. Surface Wave Characteristics of Fluid-Loaded Multilayered Media

(Included as an attachment in the form of a manuscript)

III. Publications of Research Sponsored by This Grant

Several publications comprising extensive comparisons between our theoretical and numerical model and the experimental results of Dr. D. Chimenti at the Material Laboratory have resulted. These include:

Nayfeh, A.H., "Ultrasonic Reflections from Water-Laminated Composite Intefaces," to appear in Journal of Applied Physics, January, 1988.

Nayfeh, A.H. and Chimenti, D.E., "Propagation of Guided Waves in Fluid-Coupled Plates of Fiber-Reinforced Composite," to appear in Journal of Acoustical Society of America, 1988.

Nayfeh, A.H., and Taylor, T.W., "Interaction of Ultrasonic Waves with Layered Media," Acousto-Ultrasonics: Theory and Application, Edited by J.C Duke, 1988.

Nayfeh A.H., and Taylor, T.W., "The Influence of Interfacial Conditions on the Ultrasonic Wave Interaction with Multilayered Media," to appear in Review of Progress in Quantitative NDE, Edited by D.O. Thompson, and D.E. Chementi, Plenum Press, 1988.

Chimenti,D.E., and Nayfeh, A.H., "Influence of Fiber Orientation on Leaky Waves in Composite Plates," to appear in Review of Progress in Quantitative NDE, Edited by D.O. Thompson and D.E. Chimenti, Plenum, 1988.

Shaikh, N., Chimenti, D.E., and Nayfeh, A.H., "Leaky Rayleigh Waves on Surfaces With Laminated Microstructure", to appear in Proceedings of the IEEE, 1988.

IV. Presentations of Research Sponsored By this Grant

All of the above quoted proceedings publications were presented at their respective conferences.

V. Abstracts Submitted for Publication During 1987

A. H. Nayfeh, T. W. Taylor and D. E. Chimenti, " Theoretical Ultrasonic Reflection and Guided Wave Propagation in Fibrous Composite Laminates ", To be presented at the Applied Mechanical and Engineering Science Conference, to be held at Berkely, California, June 20-22, 1988.

D. E. Chimenti, and A. H. Nayfeh, " Experimental Ultrasonic Reflection and Guided Wave Propagation in Fibrous Composite Laminates ", to be presented at the Applied Mechanics and Engineering Science Conference, to be held at Berkely, California, June 20-22, 1988.

A. H. Nayfeh and T. W. Taylor, " Distribution of Stresses and Displacements in Multilayered Media ", to be presented at the ASME annual meeting in Chicago, Ill. Nov. 28-Dec. 2, 1988.

VI. Work in Progress

We have started modeling the interactions of multilayered fibrous composite plates with ultrasonic waves. Arbitrary numbers of plate constituents will be allowed. All appropriate interfacial conditions will be invoked. Furthermore, in order to simulate the existance of large cracks in the forms of debonding or delaminations we plan to introduce a slip boundary condition. This condition does not require the continuity of shear stress and displacements along the interface. Thus the shear stresses on the interface will vanish and hence result in the weakening of the interface. This concept seems to be promising and will be verified experimentally in the near future. Results on this problem will be available for comparisons with the concurrently acquired experimental data of Dr. Chimenti.

VII. Professional Personnel

The grant supports Mr. Timothy Taylor who is a graduate student in the Engineering Mechanics program of the Aerospace Department. He has passed his Ph.D. qualifying examination and is now enrolled into the Ph.D. program.

Appendix A

$$C_{11} = C'_{11}G^4 + C'_{22}S^4 + 2(C'_{12} + 2C'_{66})S^2G^2$$

$$C_{12} = (C'_{11} + C'_{22} - 4C'_{66})S^2G^2 + C'_{12}(S^4 + G^4)$$

$$C_{13} = C'_{13}G^2 + C'_{23}S^2$$

$$C_{16} = (C'_{11} - C'_{12} - 2C'_{66})SG^3 + (C'_{12} - C'_{22} + 2C'_{66})GS^3$$

$$C_{22} = C'_{11}S^4 + 2(C'_{12} + 2C'_{66})S^2G^2 + C'_{22}G^4$$

$$C_{23} = C'_{23}G^2 + C_{13}S^2$$

$$C_{26} = (C'_{11} - C'_{12} - 2C'_{66})GS^3 + (C'_{12} - C'_{22} + 2C'_{66})SG^3$$

$$C_{33} = C'_{33}$$

$$C_{36} = (C'_{23} - C'_{13})SG$$

$$C_{45} = (C'_{44} - C'_{55})SG$$

$$C_{44} = C'_{44}G^2 + C'_{55}S^2$$

$$C_{55} = C'_{55}G^2 + C'_{44}S^2$$

$$C_{66} = (C'_{11} + C'_{22} - 2C'_{12} - 2C'_{66})S^2G^2 + C_{66}(S^4 + G^4)$$

Where $G = \cos\phi$ and $S = \sin\phi$.

Appendix B

Expanding the determinant relation (9) and collecting powers of α we have

$$\alpha^6 + A_1\alpha^4 + A_2\alpha^2 + A_3 = 0$$

where:

$$A_1 = (P_1F_{11} + P_2C_{55} - P_4F_{12} - P_5C_{45} + P_7F_{13})/\Delta$$

$$A_2 = (P_2F_{11} + P_3C_{55} - P_5F_{12} - P_6C_{45} + P_8F_{13})/\Delta$$

$$A_3 = (P_3F_{11} - P_6F_{12})/\Delta$$

$$\Delta = P_1C_{55} - P_4C_{45}$$

$$P_1 = C_{44}C_{55} \; ; \; P_3 = F_{22}F_{33}$$

$$P_2 = F_{23}C_{33} + F_{33}C_{44} - F_{23}$$

$$P_4 = C_{33}C_{45} \; , \; P_6 = F_{12}F_{32}$$

$$P_5 = C_{33}F_{12} + F_{33}C_{45} - F_{13}F_{23}$$

$$P_6 = F_{23}C_{45} - F_{13}C_{44} \; ; \; P_7 = F_{12}F_{23} - F_{13}F_{22}$$

$$F_{11} = C_{11} - \rho c^2$$

$$F_{12} = C_{16}$$

$$F_{13} = C_{13} + C_{55}$$

$$F_{22} = C_{66} - \rho c^2$$

$$F_{23} = C_{36} + C_{45}$$

$$F_{33} = C_{55} - \rho c^2$$

REFERENCES

1. M. J. P. Musgrave, Crystal Acoustics (Holden Day, San Francisco, 1970).
2. J. L. Synge, J. Math. Pys. 25, 323-334 (1957).
3. F. I. Fedorov, Theory of Elastic Waves in Crystals (Plenum, New York, 1968).
4. L.G. Merkulov, Appl. Mater. Res. 2, 231-240 (1963).
5. L.G. Merkulov and L.A. Yakovlev, Sov. Phys. Acoust. 8, 72-77 (1962).
6. L.G. Merkulov and L.A. Yakovlev, Sov. Phys. Acoust. 8, 152-155 (1962)
7. M.J.P. Musgrave, Geophys. J. 3, 406-418 (1960)
8. E. Gates, Appl. Phys. Lett. 7, 187-189 (1965).
9. N. Joel, Proc. Phys.Soc, Sect. A 78, 38 (1961).
10. E.G. Henneke, II,J. Acoust. Soc. Am. 51, 210 (1972).
11. T.C. Lim and M.J.P. Musgrave, Nature 225, 372 (1970).
12. W.W. Johnson,Bull. Seismol. Soc. Am. 60, 11005 (1970).
13. P.Chadwick and P.K. Currie, Q.J. Mech. Appl. Math XXVII, 497 (1974).
14. S.I. Rokhlin, T.K. Bolland and Laszlo Adler, J. Acoust. Soc. Am. 79(4), 906-918 (1986)
15. R. Stonley, Proc. Lond. Math. Soc. 232, 447 (1955).
16. V.T. Buchwald, Q.J. Mech. Appl. Math. 14, 461 (1961).
17. V.T. Buchwald and A. Davis, Nature (Lond.) 191, 899 (1961).
18. V.T. Buchwald and A. Davis, Q. J. Mech.Appl. Math 16 283 (1963).
19. D.C. Gazis, R. Herman, and R.F. Wallis, Phys. Rev. 119, 533 (1960).
20. F.R. Rollins, T.C. Lim, and G.W. Farnell, Appl. Phys. Lett. 12, 236 (1968).
21. T.C. Lim and G.W. Farnell, J. Acoust. Soc. Am. 45, 845 (1969).

22. See, for example, the series Physical Acoustics, ed. by W.P. Mason and,R. N. Thurston (Academic Press, New York).

23. S.A. Markus, M.D. Kaplan, and S.V. Veremeenko, Defektoskopiya 21, 3 (1985) [Sov.J. Nondestr. Test. 21 739 (1985)].

24. Zh. G. Nikiforenko, V. T. Bobrov, and I. I. Averbukh, Defektoskopiya 8, 56 (1972) [Soc. J. Nondestr. Test. 8, 543 (1972)].

25. I. Abubakar, Quart. J .Mech. and Appl. Math. (Part I), 15, 29 (1962)

26. Yu. A. Kosevich and E. S. Syrkin, Sov. Phys. Acoust. 31, 365 (1985).

27. E.R. Baylis and W. A. Green, Journal of Sound and Vibration 110(1),1-26 (1986).

28. L. G. Merkulov and D. A. Tursonov, Sov. Phys. Acoust. 15, 115 (1969).

29. L. P. Solie and B. A. Auld, J. Acoust. Soc. Am. 54(1), 50-65, (1973).

30. D. E. Chimenti and A. H. Nayfeh, J. Appl. Phys. 58 4531 (1985).

31. A. H. Nayfeh and D.E. Chimenti, submitted to J. Acous. Soc. Am..

32. L. M. Brekhovskikh, Waves in Layered Media, (Academic Press, New York, 1960).

33. I. A. Viktorov, Rayleigh and Lamb Waves, (Plenum,New York, 1967).

34. H. Lamb, Proc. Roy. Soc. (London), Ser. A, 93, 114 (1917).

35. C'_{11}, C'_{22}, C'_{33}, C'_{13}, C'_{23}, C'_{44}, C'_{55} are given by 155.6, 11.5, 15.95, 3.72, 4.33, 5.81, 6.5 GPa, respectively, ρ = 1.6 g/cm^3, c_f = 1.48 km/sec and ρ_f = 1 g/cm^3.

36. D.E. Chimenti and A.H. Nayfeh, Appl. Phys. Letters 49, 492 (1986).

37. L. Cremer, Akust. Z. 7, 81 (1942).

38. M. Knight, J. Composite Mat. 16, 153 (1982).

39. W. Prosser, Ph.D. Thesis, Johns Hopkins Univ., 1987 (unpublished).

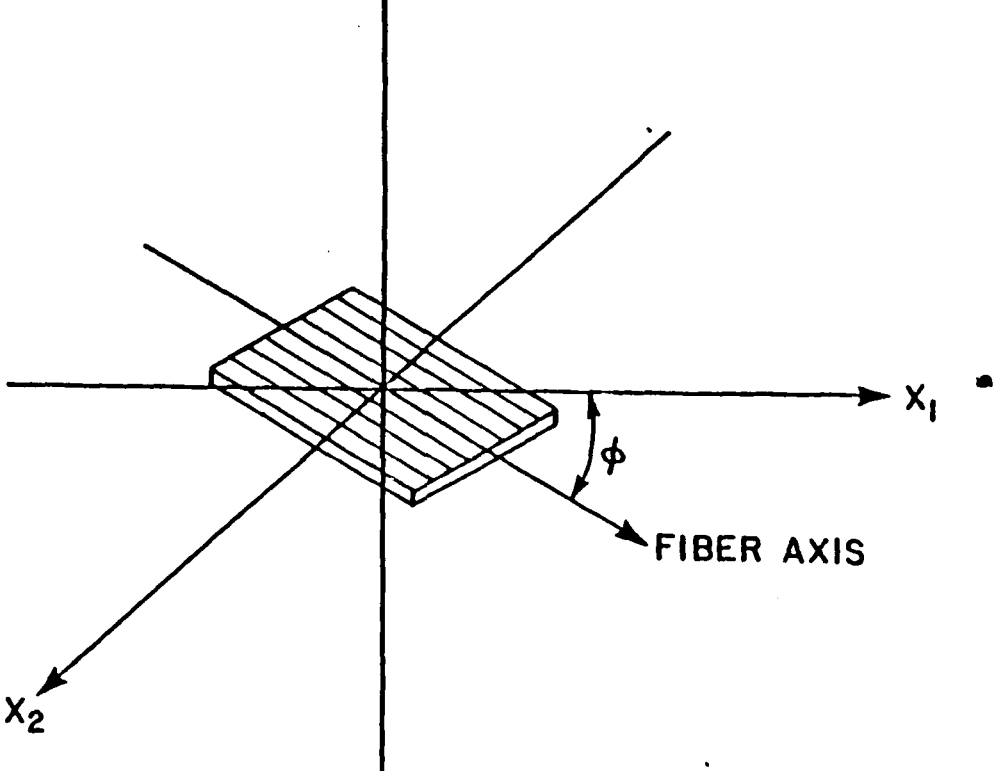

Figure 1. Coordinate system for leaky plate wave problem. Incident beam strikes plate at angle θ, and ϕ is angle between fiber axis and plane of incidence.

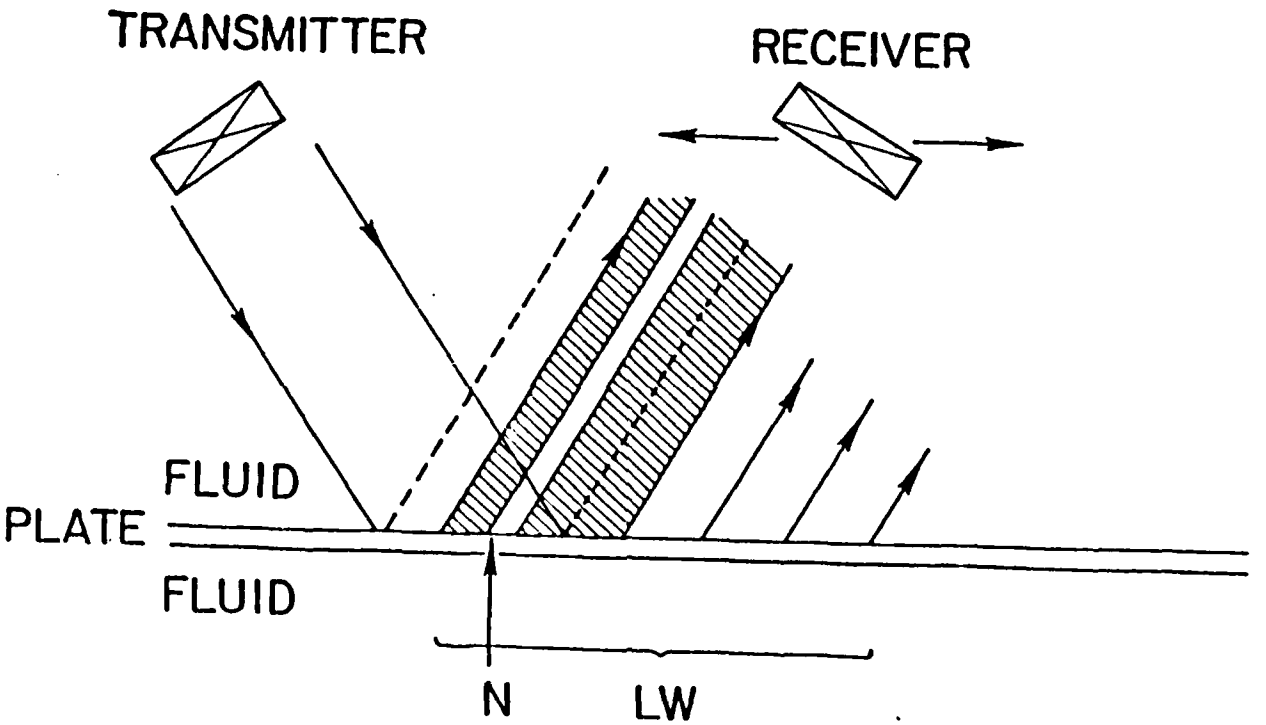

Figure 2. Experimental geometry of ultrasonic reflection measurements in fibrous composite plates. Transmitter is fixed with respect to the sample, while receiver is scanned parallel to interface. Dashed lines show specular reflection. When plate wave is excited, reflected energy is redistributed as indicated. Null zone is denoted by N, and LW stands for leaky wave field. A similar radiation pattern exists below the plate.

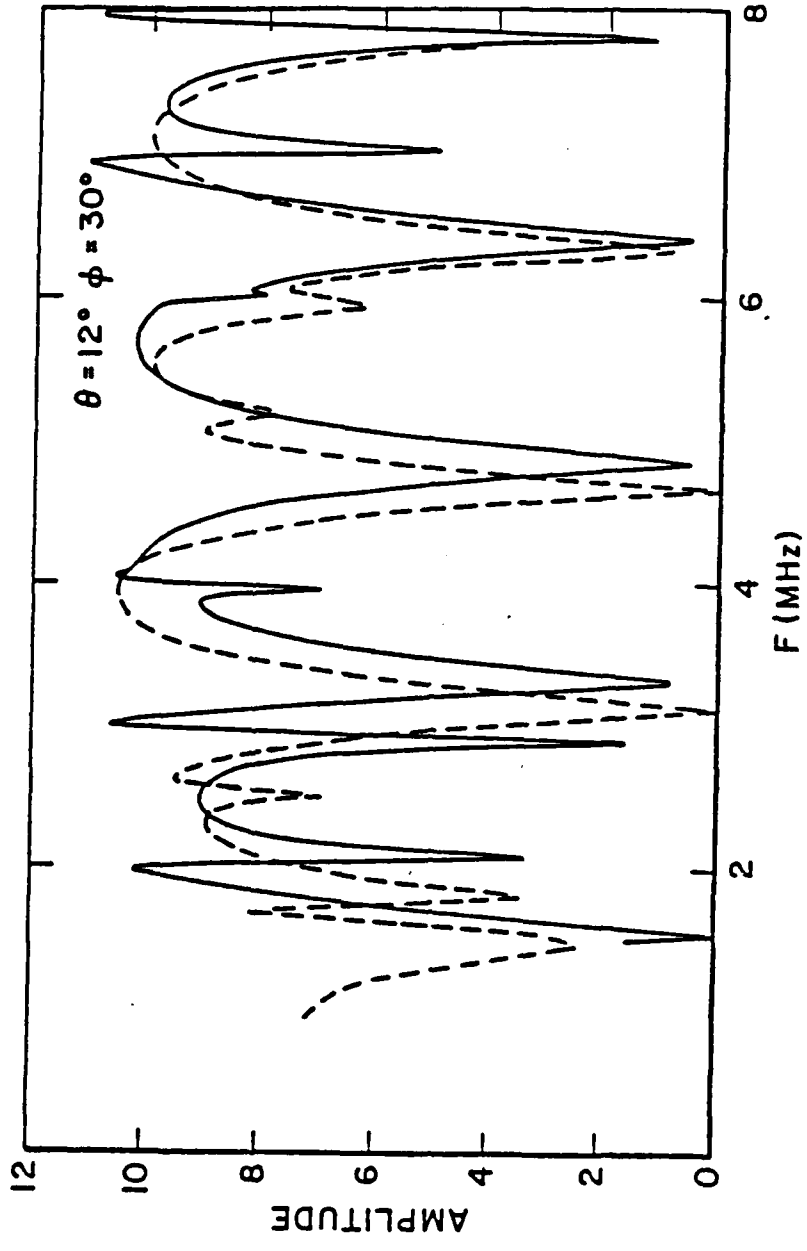

Figure 3(a). Reflection (plate-wave) spectrum for $\theta = 12°$ and $\phi = 30°$. Theory is solid curve and experiment is dashed curve. Data has been deconvolved to remove transducer response.

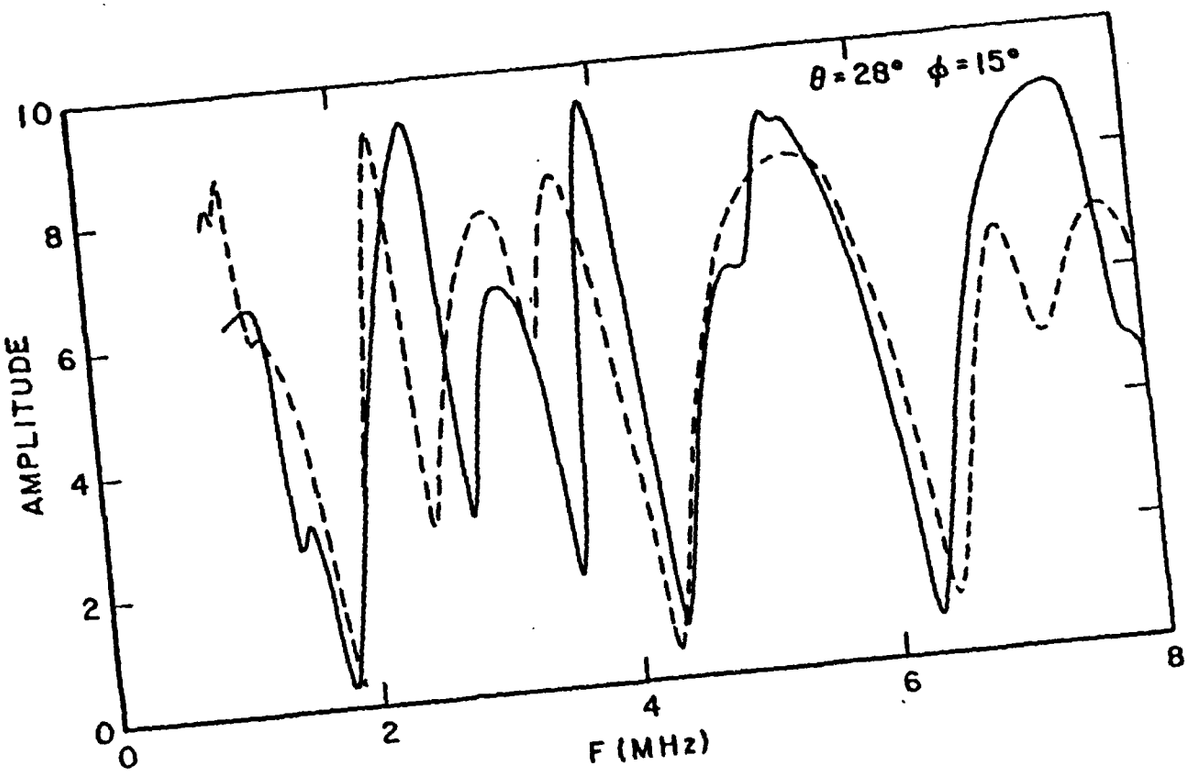

Figure 3(b). Reflection spectrum for $\theta = 28°$ and $\phi = 15°$.

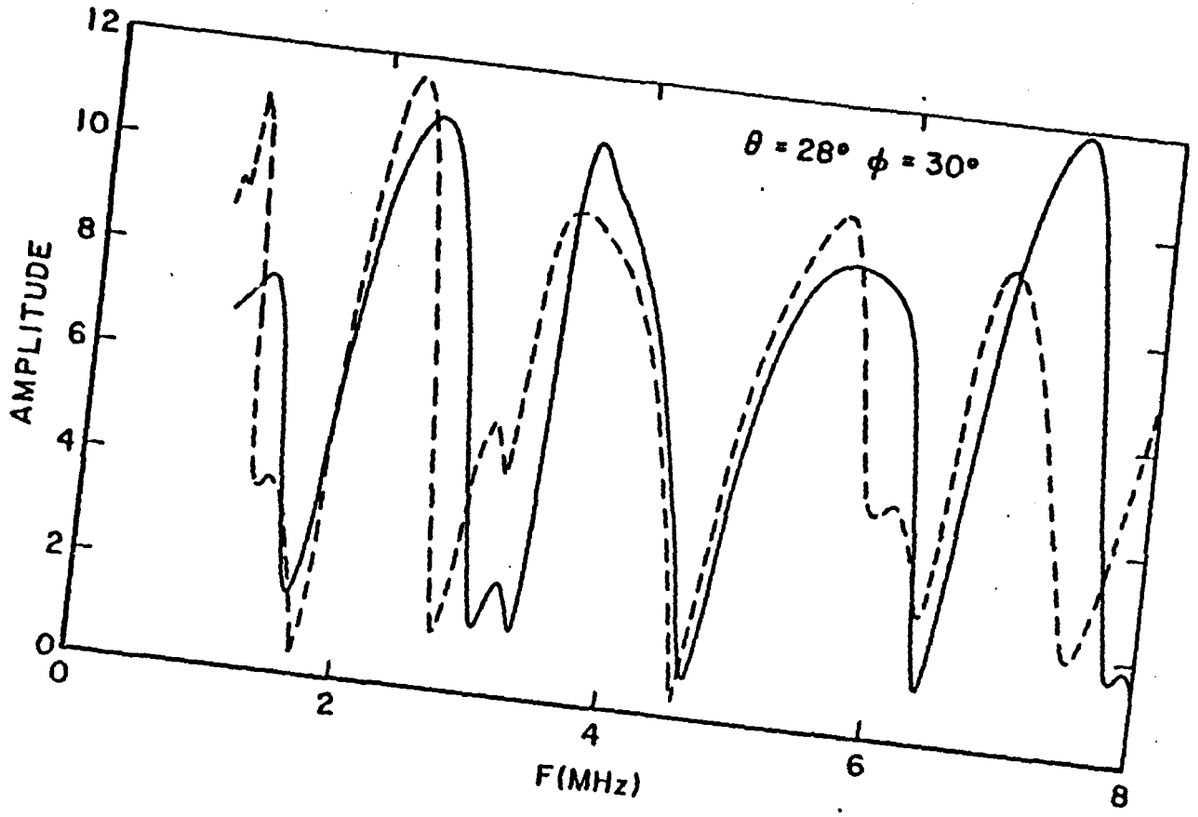

Figure 3(c). Reflection spectrum for $\theta = 28°$ and $\phi = 30°$.

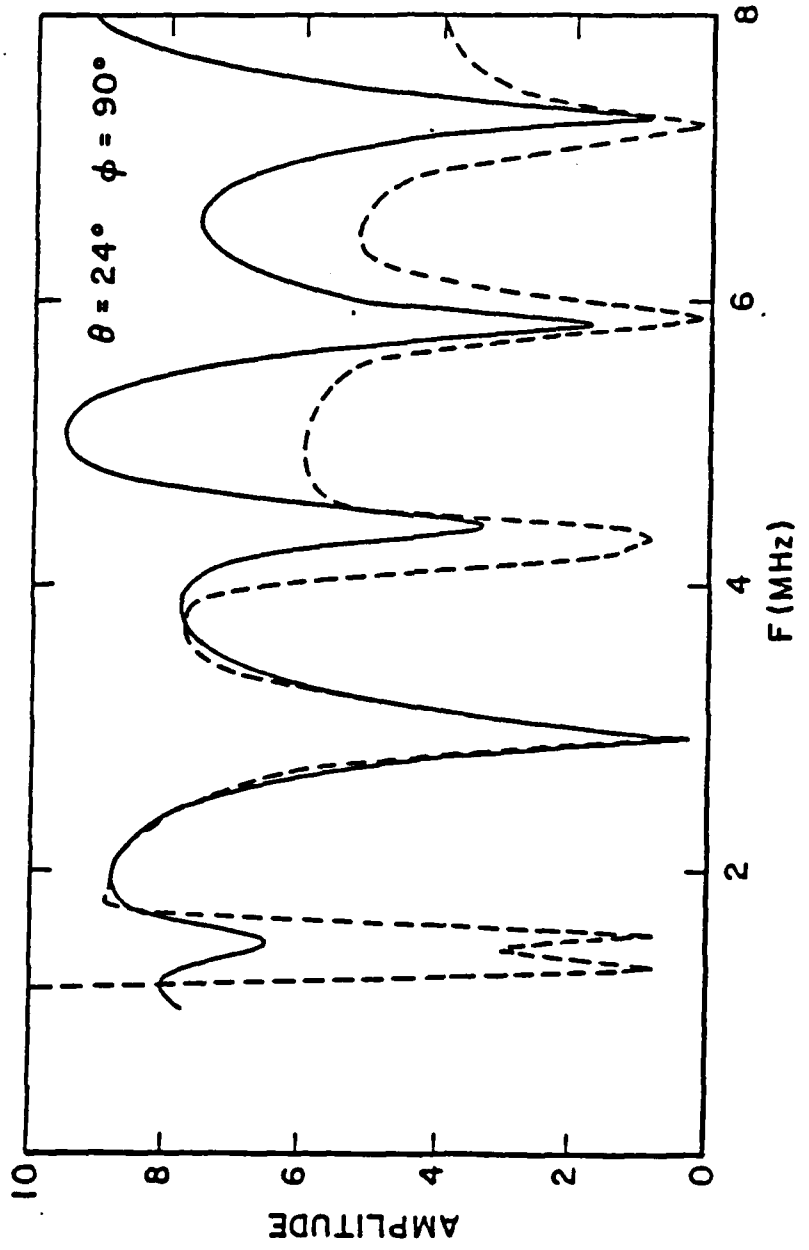

Figure 3(d). Reflection spectrum for θ = 24° and φ = 90°.

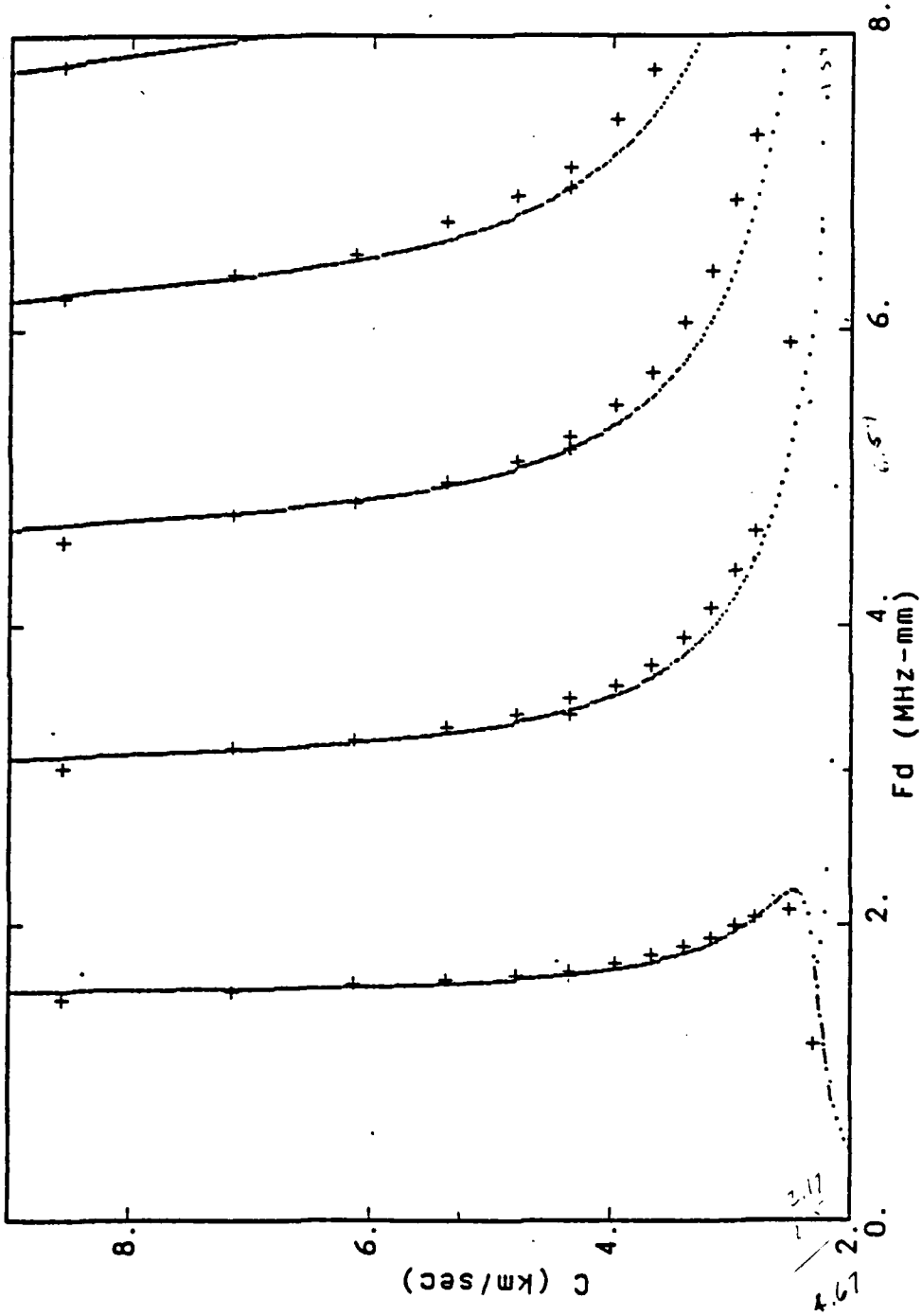

Figure 4(a). Reflection results expressed as phase velocity dispersion curves for $\phi = 0°$. Data are plotted as discrete crosses; theory curves are small filled circles. In some regions of the theory curves dashed lines have been added as a guide to the eye.

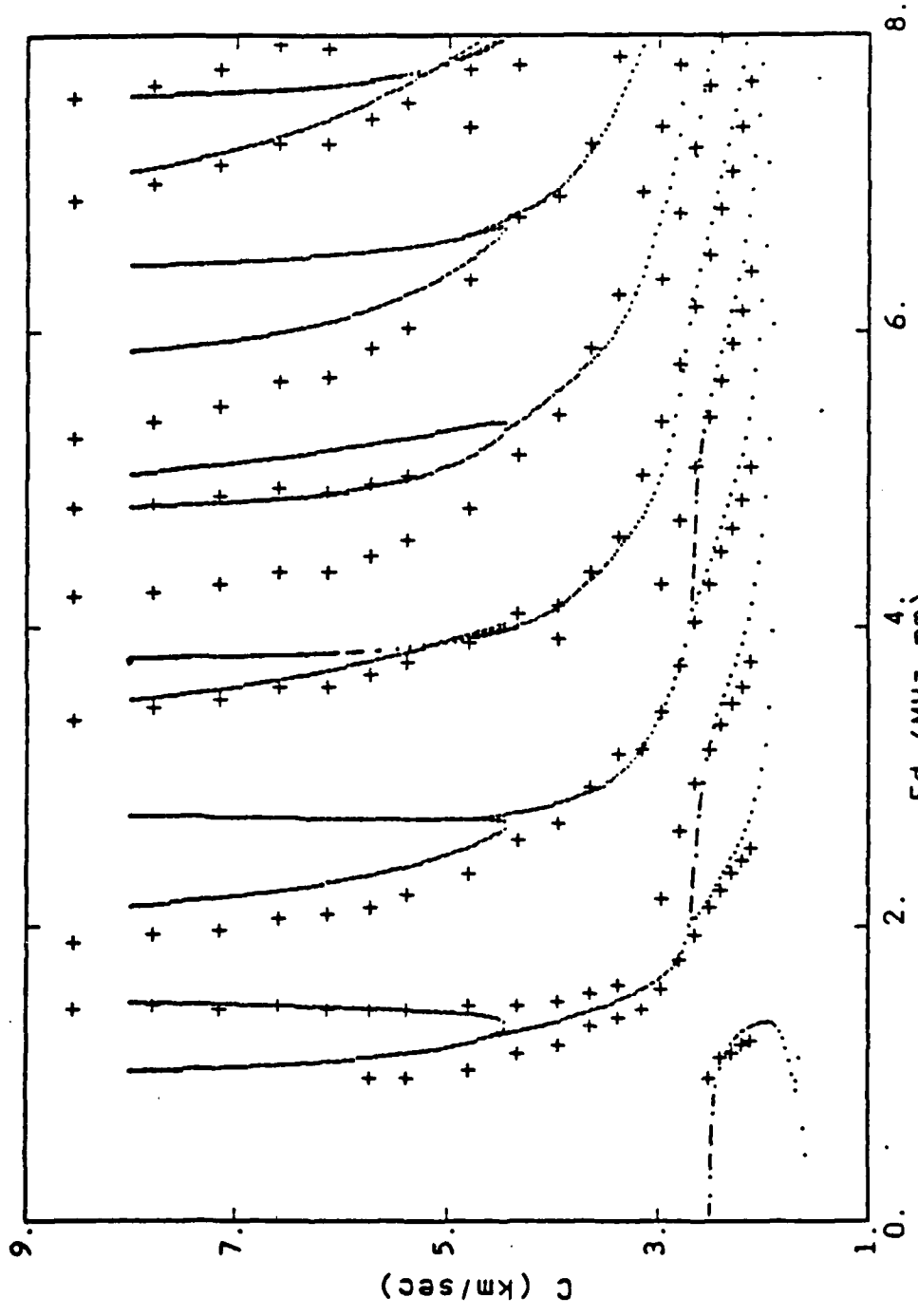

Figure 4(b). Dispersion plot for $\phi = 90°$. Data are crosses; theory curves are small filled circles.

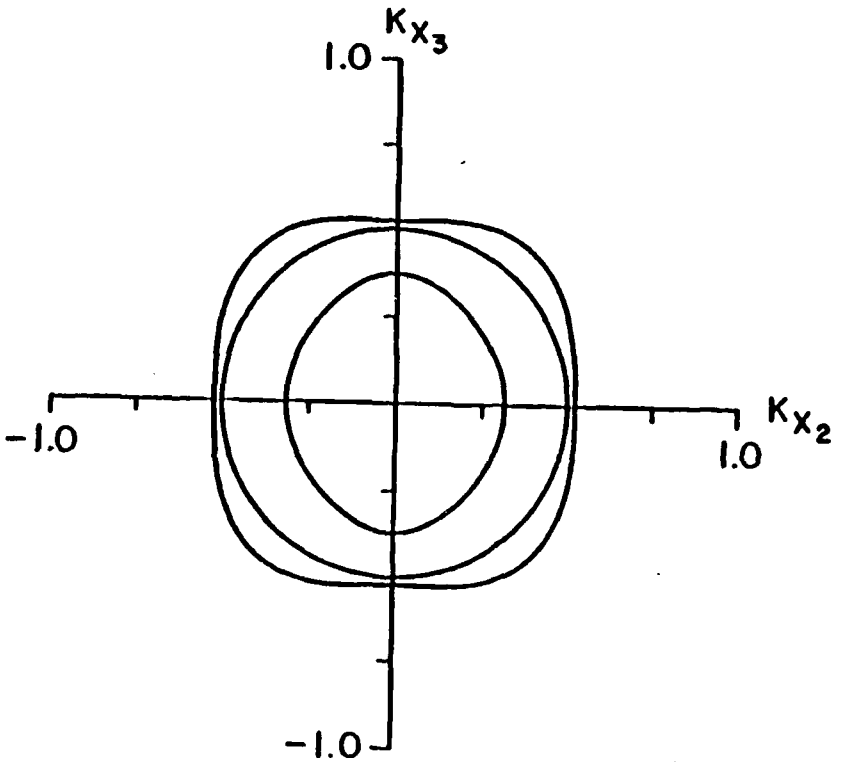

Figure 5. Slowness curves with the elastic constants of Ref. [35] for $\phi = 90°$. Anisotropy in this plane is due to orthotropic nature of plate studied. Fast quasitransverse wave is still seen to be isotropic.

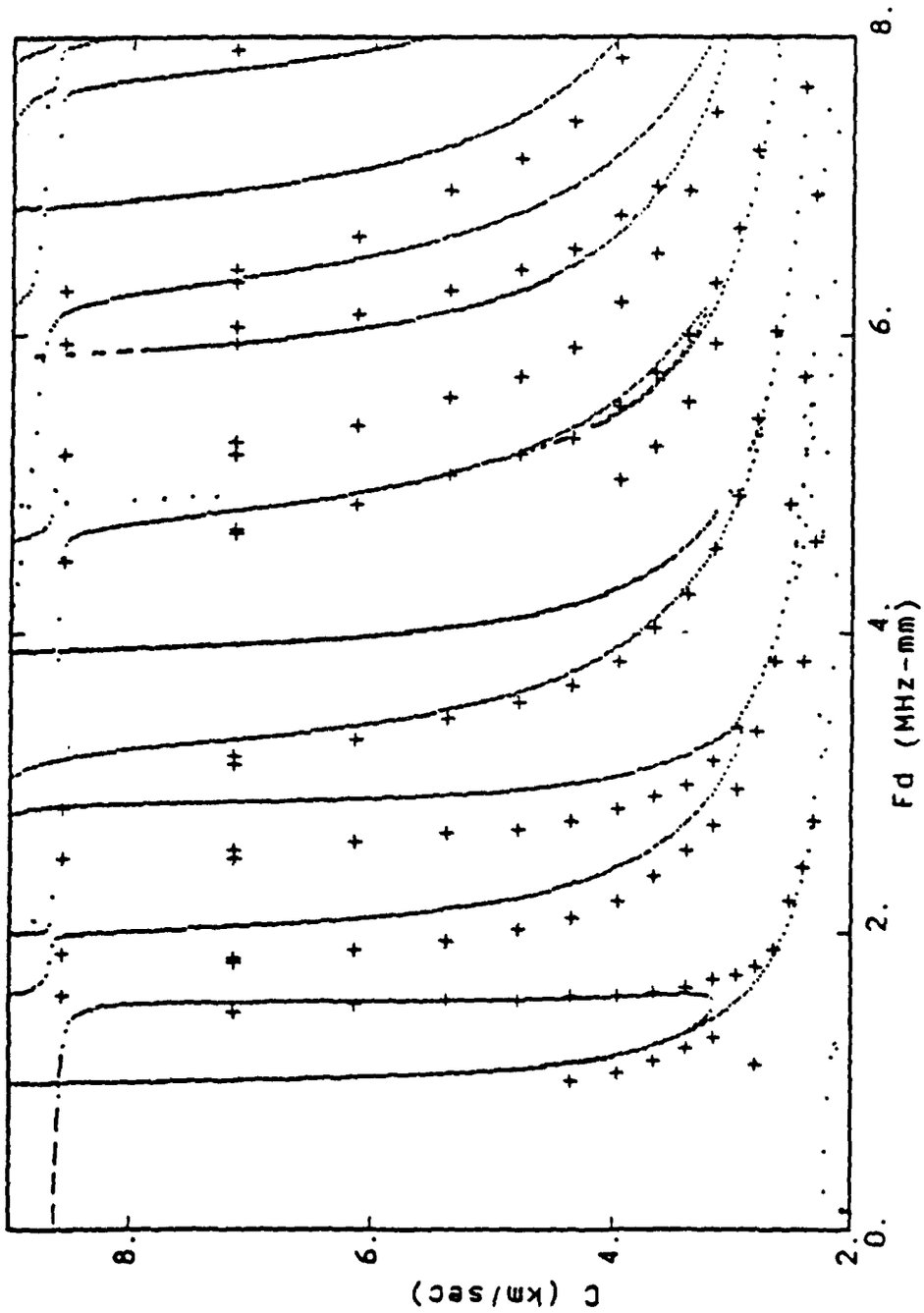

Figure 6(a). Dispersion plot for $\phi = 30°$.

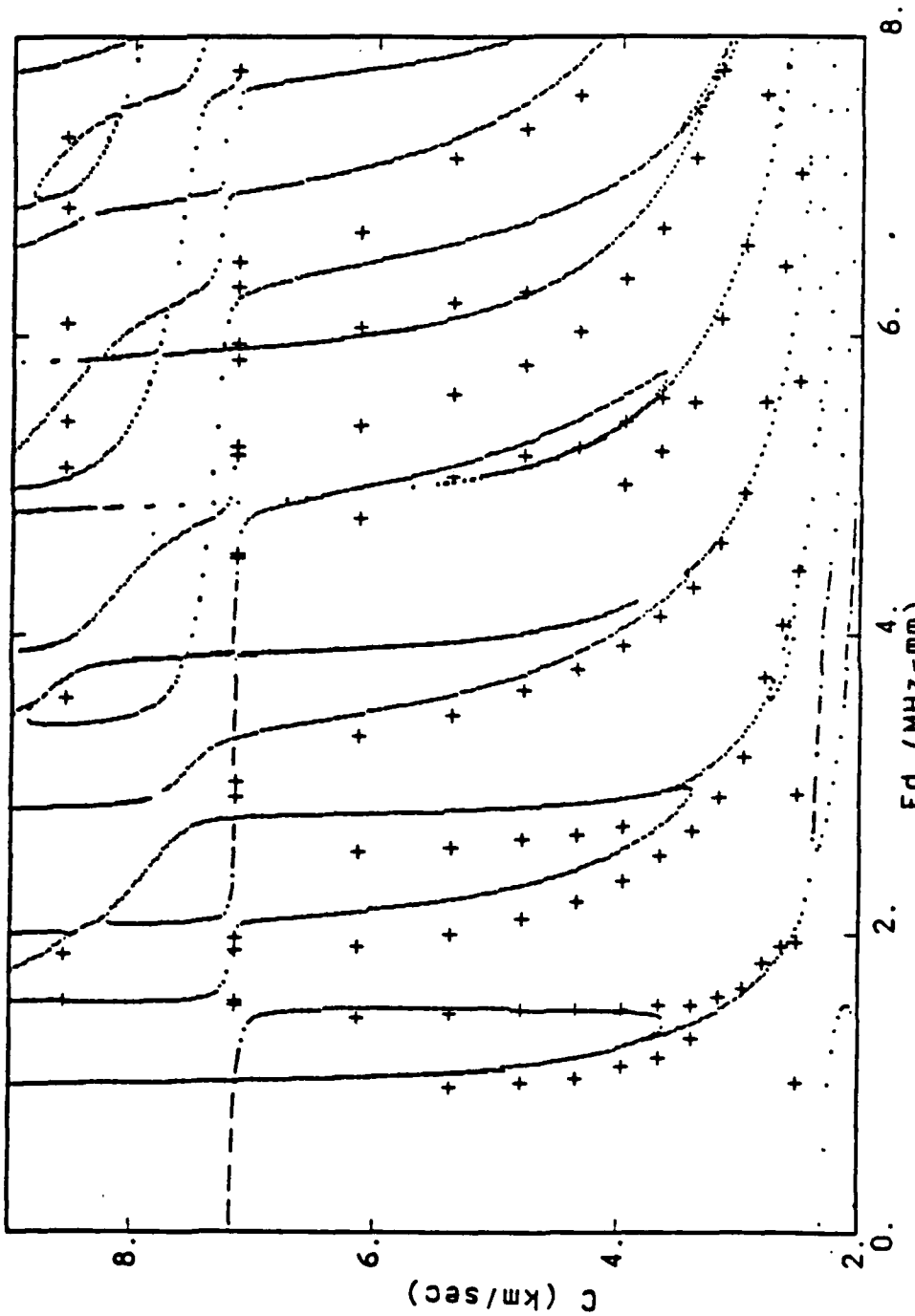

Figure 6(b). Dispersion plot for ϕ = 45°.

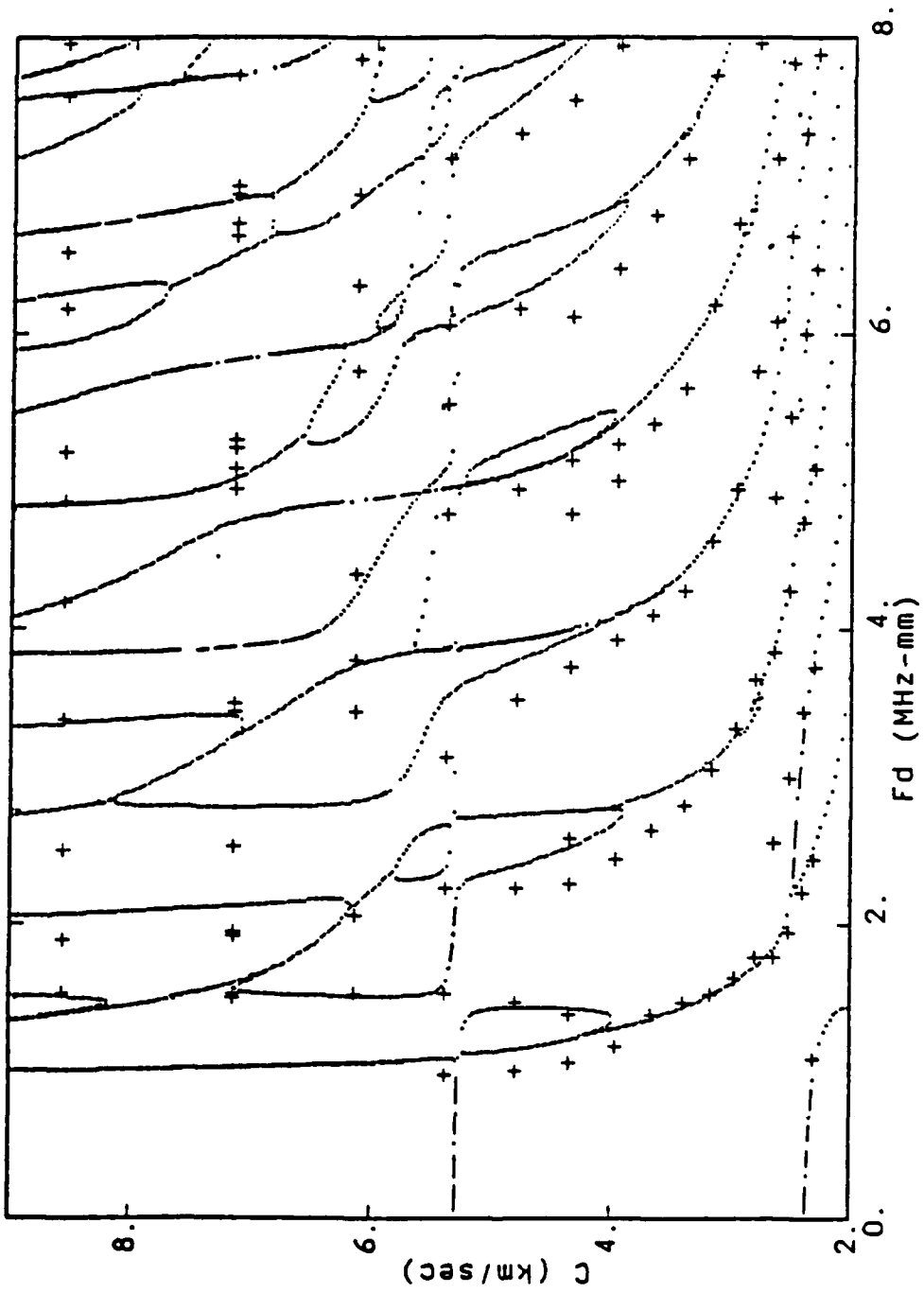

Figure 6(c). Dispersion plot for $\phi = 60°$.

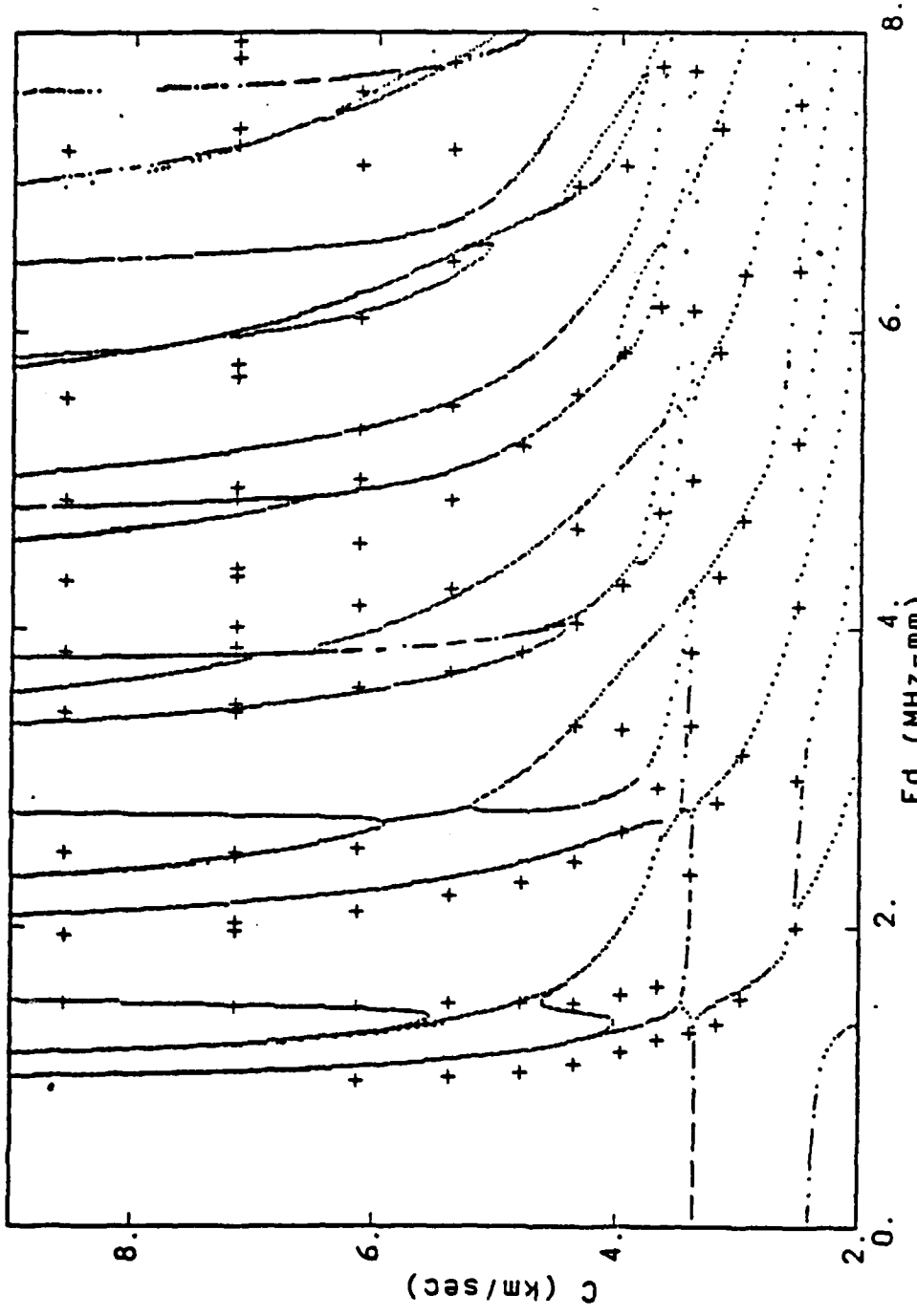

Figure 6(d). Dispersion plot for $\phi = 75°$.

"SURFACE WAVE CHARACTERISTICS OF FLUID-LOADED MULTILAYERED MEDIA"

by

Adnan H. Nayfeh*

Timothy W. Taylor**

University of Cincinnati

Cincinnati, OH 45221

Abstract

A unified theoretical treatment is presented for the interaction of ultrasonic waves with multilayered media. The wave is supposed to be incident from water, at an arbitrary angle, upon a plate consisting of an arbitrary number of different material layers. The composite plate is supported from the bottom by a solid half-space. It is assumed that all solid interfaces are either rigidly or smoothly bonded. The smooth contact interface condition is of special importance since it may simulate weak bondings, extended cracks, or delaminations; such situations are of great interest for nondestructive evaluation applications. Reflection and transmission coefficients are derived for the total system. By examining the behavior of the reflection coefficient, all of the propagating modes are identified. Furthermore, the rate of energy leakage in the fluid is derived. Extensive numerical results are given in order to delineate the influence of the plate material orderings on the propagation process. Included are also comparisons of results obtained under the rigid and the smooth bonding assumptions.

* Professor

** Graduate Assistant

I. INTRODUCTION

The lateral displacement and associated distortion of a bounded acoustic beam upon its reflection from fluid-solid interfaces have been the subject of many analytical and experimental investigations [1-15]. Although these effects are found to exist for any angle of incidence, the beam suffers severe distortion if it is incident at, or near, the Rayleigh critical angle. Physically, resonant generation of a Rayleigh-like surface wave and rapid reradiation of its energy into the fluid are responsible for the severe displacement and distortion of the beam.

In three recent papers [10-13] Nayfeh and Chimenti analyzed, both analytically and experimentally, the reflected waves from liquid-solid half-spaces interfaces separated by a solid layer of different elastic material in rigid contact to the solid half-space. In [11-12] we derived exact expressions for the reflection coefficients where, as in our earlier paper [10], only an approximate expression was reported. As was discussed in these papers all physical effects of the reflected beam can be explained by examining the behavior of the appropriate reflection coefficient. Generally speaking, the inclusion of the layer was found to give rise to dispersive effects in both the surface wave speed and the lateral shifting (displacement) of the beam. These two effects are found to further influence the distortion of the reflected beam. It was also found [12] that the specific influence of the layer depends highly upon its material properties as compared to that of the substrate. Specifically, the layer can either load or stiffen the substrate. The loading situation occurs when the layer's properties (especially its shear wave speed) are smaller than those of the substrate, whereas stiffening occurs for layers stiffer than

the substrate. Here we mention that concurrent with our investigations Bogy and Gracewski conducted analyses and presented numerous results on similar problem situations [13-15].

In the present paper we generalize our single layer results to the case of an arbitrary number of layers separating the fluid and solid half-spaces. Among its many applications it can be used to examine the combined influence of loading and softening layers. This is of particular importance in advanced device applications where there is a need for characterizing material properties of material deposition (in the forms of thin layers) on host substrates.

In order to generalize our single layer's result to the multilayer case we use the matrix transfer technique introduced originally by Thomson [16] and somewhat later on by Haskell [17] and others [18-23] for applications in the geophysics, acoustic and electromagnetic fields. According to this technique we construct the propagation matrix for a stack of arbitrary number of layers by extending the solution from one layer to the next while satisfying the appropriate interfacial continuity conditions.

In order to execute our results we shall carry out our analysis in terms of the displacements and stresses directly rather than in terms of the wave potentials. This leads to somewhat simpler expressions and is also chosen as a prelude to our future development of similar analysis for anisotropic media. In order to simulate a wide variety of debonding, delamination and cracking, we shall introduce a new feature which allows us to treat "smooth" interfacial conditions at selectively arbitrary locations. These conditions can be simulated by introducing a very thin layer (of negligible thickness) of nonviscous fluid between solid interfaces, or by

setting the smooth interfaces in contact without bonding. As a result, transverse slip occurs at the boundary resulting in the vanishing of the shear stresses at the interface for both media. On the other hand, the components of displacements and stresses normal to the interface plane are kept continuous as if the media were in rigid contact.

In Section II we present complete analysis for the multilayered system with all rigidly bonded interfaces. This will result in algebraic expressions for the reflection and the transmission coefficients. In Section III, we invoke the smooth interface condition at the arbitrary interface between layer m and m+1 of the plate and thus modify the reflection and transmission coefficients accordingly. In seciton IV we present a qualitative description of leaky mode extraction. In section V, we present a wide variety of numerical results to delineate the utility of the models. Several comparisons between results obtained under the rigid or the smooth interfacial conditions assumptions will be presented.

II. THEORETICAL DEVELOPMENTS CASE OF RIGID BONDS

(a) Formulation of the Problem

Consider a laminated plate consisting of an arbitrary number, n, of elastic isotropic layers rigidly bonded at their interfaces. This plate is assumed to be rigidly attached to an elastic isotropic solid half-space separating it from a fluid half-space. The problem then is to study the reflected beam from the fluid-plate interface for an incident beam originating in the fluid at an arbitrary angle from the normal to the interface.

Guided by our single layer plate analysis of [12], in order to facilitate the present analysis, we shall use two sets of two-dimensional

coordinate systems (x,z), as illustrated in figure 1. One system is global which has its origin at the substrate-plate interface such that x denotes the propagation direction and z is normal to the interfaces. Here the layered plate will then occupy the space $0 \leq z \leq d$ where d denotes the total thickness of the plate. The second system is local for each sublayer of the plate. Since the plate is made of n layers, the kth layer will then have its local coordinates x and $z^{(k)}$ with local origin at the interface between layers k-1 and k. Hence layer k occupies the space $0 \leq z^{(k)} \leq d^{(k)}$, where $d^{(k)}$ is its thickness. In figure 2 we display a representative layer k with its appropriate coordinates and boundary field variables.

With this choice of coordinate systems all motions will be independent of the y-direction and the relevant elastodynamic equations for each solid (including each layer and the substrate) consist of the momentum equations

$$\frac{\partial \sigma_x}{\partial x} + \frac{\partial \sigma_{xz}}{\partial z} = \rho \frac{\partial^2 u}{\partial t^2} \tag{1}$$

$$\frac{\partial \sigma_z}{\partial z} + \frac{\partial \sigma_{xz}}{\partial x} = \rho \frac{\partial^2 w}{\partial t^2} \tag{2}$$

and the constitutive relations

$$\sigma_x = (\lambda + 2\mu)\frac{\partial u}{\partial x} + \lambda \frac{\partial w}{\partial z} \tag{3}$$

$$\sigma_z = (\lambda + 2\mu)\frac{\partial w}{\partial z} + \lambda \frac{\partial u}{\partial x} \tag{4}$$

$$\sigma_{xz} = \mu\left(\frac{\partial u}{\partial z} + \frac{\partial w}{\partial x}\right) \tag{5}$$

where σ_x, σ_{xz} and σ_z are the components of the stress tensor; u and w are the components of the displacements; ρ, λ and μ are the density and elastic constants of each material. Due to the absence of viscosity in the fluid

(water) its relevant field equations corresponding to equations (1-5) are given by

$$\frac{\partial \sigma_x^{(f)}}{\partial x} = \rho_f \frac{\partial^2 u^{(f)}}{\partial t^2} , \tag{6a}$$

$$\frac{\partial \sigma_z^{(f)}}{\partial z} = \rho_f \frac{\partial^2 w^{(f)}}{\partial t^2} \tag{6b}$$

$$\sigma_z^{(f)} = \sigma_x^{(f)} = \lambda_f \left(\frac{\partial u^{(f)}}{\partial x} + \frac{\partial w^{(f)}}{\partial z} \right) \tag{7}$$

Equations (1-7) must be supplemented with the appropriate interfacial continuity conditions. For rigid bonding between the individual layers of the plate these are

$$\sigma_{xz}^{(k)} = \sigma_{xz}^{(k+1)}, \quad \sigma_z^{(k)} = \sigma_z^{(k+1)}$$

$$u^{(k)} = u^{(k+1)}, \quad w^{(k)} = w^{(k+1)}, \quad k = 1,2,\ldots,n-1 \tag{9}$$

at $z^{(k)} = d^{(k)}$ (or $z^{(k+1)} = 0$)

Similarly, at the substrate's interface the rigid bonding continuity conditions are given by

$$\sigma_{xz}^{(1)} = \sigma_{xz}^{(s)}, \quad \sigma_z^{(1)} = \sigma_z^{(s)}$$

$$u^{(1)} = u^{(s)}, \quad w^{(1)} = w^{(s)} \tag{10}$$

at $z^{(1)} = 0$ (or global $z = 0$). Here superscript (s) designates the substrate. Finally, at the fluid-plate interface, the appropriate bonding conditions are

$$\sigma_{xz}^{(n)} = 0, \quad \sigma_z^{(n)} = \sigma_z^{(f)}, \quad w^{(n)} = w^{(f)} \tag{11}$$

at $z^{(n)} = d^{(n)}$ (or global $z = d$)

(b) Analysis

In this subsection we shall describe the propagation process in the plate by solving the field equations in each of its layers and satisfying the interfacial continuity conditions. By combining equations (1-7) we obtain the following two coupled displacement equations, which hold in each layer of the plate, as well as in the substrate

$$[(\lambda + 2\mu)\frac{\partial^2}{\partial x^2} + \mu\frac{\partial^2}{\partial z^2} - \rho\frac{\partial^2}{\partial t^2}]\, u + (\lambda+\mu)\frac{\partial^2 w}{\partial x \partial z} = 0 \tag{12}$$

$$(\lambda + \mu)\frac{\partial^2 u}{\partial x \partial z} + [(\lambda + 2\mu)\frac{\partial^2}{\partial z^2} + \mu\frac{\partial^2}{\partial x^2} - \rho\frac{\partial^2}{\partial t^2}]\, w = 0 \tag{13}$$

For waves whose projected wave vector is along the x-axis, equations (12) and (13) admit the formal solutions

$$(u,w) = (U,W)e^{iq(x-ct+\alpha z)} \tag{14}$$

where U and W are constant amplitudes, q is the wave number, c is the phase velocity and α is the ratio of the z and x-directions wave numbers. By satisfying equations (12) and (13), followed by solving for the four roots of α and using superposition we conclude that

$$\begin{vmatrix} u \\ w \end{vmatrix} = \begin{vmatrix} 1 & 1 & 1 & 1 \\ \alpha_1 & -\alpha_1 & -\frac{1}{\alpha_2} & \frac{1}{\alpha_2} \end{vmatrix} \begin{vmatrix} U_1\, e^{iq\alpha_1 z} \\ U_2\, e^{-iq\alpha_1 z} \\ U_3\, e^{iq\alpha_2 z} \\ U_4\, e^{-iq\alpha_2 z} \end{vmatrix} \tag{15}$$

where

$$\alpha_1^2 = \frac{c^2}{c_L^2} - 1\ ,\ \alpha_2^2 = \frac{c^2}{c_T^2} - 1 \tag{16a}$$

and for compactness, we define

$$U_j = \bar{U}_j\, e^{iq(x-ct)},\ j = 1,2,3,4 \tag{16b}$$

Here $c_L = [(\lambda+2\mu)/\rho]^{1/2}$ and $c_T = [\mu/\rho]^{1/2}$ designating longitudinal and shear wave speeds, respectively. Substituting from (15) into the stress-displacement relations (3-5), we can generalize equation (15) to also include the stresses as

$$\begin{vmatrix} u \\ w \\ \bar{\sigma}_z \\ \bar{\sigma}_{xz} \end{vmatrix} = \begin{vmatrix} 1 & 1 & 1 & 1 \\ \alpha_1 & -\alpha_1 & -\frac{1}{\alpha_2} & \frac{1}{\alpha_2} \\ D_1 & D_1 & D_2 & D_2 \\ D_3 & -D_3 & D_4 & -D_4 \end{vmatrix} \begin{vmatrix} U_1 e^{iq\alpha_1 z} \\ U_2 e^{-iq\alpha_1 z} \\ U_3 e^{iq\alpha_2 z} \\ U_4 e^{-i\alpha_2 z} \end{vmatrix} \tag{17}$$

where

$$D_1 = \mu\left(\frac{c^2}{c_T^2} - 2\right), \quad D_2 = -2\mu$$

$$D_3 = 2\mu\alpha_1 \quad , \quad D_4 = \frac{\mu}{\alpha_2}\left(\frac{c^2}{c_T^2} - 2\right),$$

$$\bar{\sigma}_z = \sigma_z/iq \text{ and } \bar{\sigma}_{xz} = \sigma_{xz}/iq \tag{18}$$

Since equations (12)-(18) hold for each layer k (k = 1,...,n), equation (17) can be used to relate the displacements and stresses at $z^{(k)} = 0$ to those at $z^{(k)} = d^{(k)}$. This can be done by specializing (17) to $z^{(k)} = 0$ and to $z^{(k)} = d^{(k)}$, and eliminating the common amplitude column made up of $U_1^{(k)}$, $U_2^{(k)}$, $U_3^{(k)}$ and $U_4^{(k)}$ resulting in

$$\begin{vmatrix} u^{(k)} \\ w^{(k)} \\ \bar{\sigma}_{xz}^{(k)} \\ \bar{\sigma}_{xz}^{(k)} \end{vmatrix}_{z^{(k)} = d^{(k)}} = \begin{vmatrix} a_{11} & a_{12} & a_{13} & a_{14} \\ a_{21} & a_{22} & a_{23} & a_{24} \\ a_{31} & a_{32} & a_{33} & a_{34} \\ a_{41} & a_{42} & a_{43} & a_{44} \end{vmatrix} \begin{vmatrix} u^{(k)} \\ w^{(k)} \\ \bar{\sigma}_z^{(k)} \\ \bar{\sigma}_{xz}^{(k)} \end{vmatrix}_{z^{(k)} = 0} \tag{19}$$

where

$$[a_{ij}]_k = \begin{vmatrix} B_1 & B_2 & B_3 & B_4 \\ \alpha_1 B_1 & -\alpha_1 B_2 & -\frac{1}{\alpha_2} B_3 & \frac{1}{\alpha_2} B_4 \\ D_1 B_1 & D_1 B_2 & D_2 B_3 & D_2 B_4 \\ D_3 B_1 & -D_3 B_2 & D_4 B_3 & -D_4 B_4 \end{vmatrix}_k \begin{vmatrix} 1 & 1 & 1 & 1 \\ \alpha_1 & -\alpha_1 & -\frac{1}{\alpha_2} & \frac{1}{\alpha_2} \\ D_1 & D_1 & D_2 & D_2 \\ D_3 & -D_3 & D_4 & -D_4 \end{vmatrix}_k^{-1} \tag{20}$$

and

$$B_1 = e^{iq\alpha_1 d^{(k)}}, \quad B_2 = e^{-iq\alpha_1 d^{(k)}}$$

$$B_3 = e^{iq\alpha_2 d^{(k)}}, \quad B_4 = e^{-iq\alpha_2 d^{(k)}} \tag{21}$$

and the various parameters α_1, α_2, D_1, etc. are specialized to the material k under consideration.

By applying the above procedure for each layer and invoking the continuity relations on the top and bottom of each layer we can finally relate the displacements and stresses at the top of layer *n* to those at the bottom of layer 1 via the transfer matrix multiplications

$$[A_{ij}] = [a_{ij}]_n [a_{ij}]_{n-1} \cdots [a_{ij}]_1 \tag{22}$$

which can be written in the expanded form

$$\begin{vmatrix} u^{(n)} \\ w^{(n)} \\ \bar{\sigma}_z^{(n)} \\ \bar{\sigma}_{xz}^{(n)} \end{vmatrix}_{z=d} = \begin{vmatrix} A_{11} & A_{12} & A_{13} & A_{14} \\ A_{21} & A_{22} & A_{23} & A_{24} \\ A_{31} & A_{32} & A_{33} & A_{34} \\ A_{41} & A_{42} & A_{43} & A_{44} \end{vmatrix} \begin{vmatrix} u^{(1)} \\ w^{(1)} \\ \bar{\sigma}_z^{(1)} \\ \bar{\sigma}_{xz}^{(1)} \end{vmatrix}_{z=0} \tag{23}$$

Now, in order to satisfy the remaining continuity conditions (10) and (11) at the substrate-plate and the plate-fluid interfaces, respectively, we need to solve the field equations in the substrate and in the fluid. By inspection, such solutions can be deduced from the formal solution (17).

First, due to the absence of shear deformation, specializing (17) to the fluid half-space yields

$$\begin{vmatrix} u^{(f)} \\ w^{(f)} \\ \bar{\sigma}_z^{(f)} \end{vmatrix} = \begin{vmatrix} 1 & 1 \\ \alpha_f & -\alpha_f \\ \rho_f c^2 & \rho_f c^2 \end{vmatrix} \begin{vmatrix} U_1^{(f)} e^{iq\alpha_f(z-d)} \\ U_2^{(f)} e^{-iq\alpha_f(z-d)} \end{vmatrix} \tag{24a}$$

where

$$\alpha_f^2 = (c^2/c_f^2) - 1, \; U_r^{(f)} = \bar{U}_r^{(f)} \, e^{iq(x-ct)}, \; r = 1,2. \tag{24b}$$

with $\bar{U}_1^{(f)}$ is the constant amplitude of the incoming wave, $\bar{U}_2^{(f)}$ is that of the reflected wave and z is the global coordinate. Also, the sub and superscripts f denote quantities belonging to the fluid.

Next, specializing (17) to the substrate yields

$$\begin{vmatrix} u^{(s)} \\ w^{(s)} \\ \bar{\sigma}_z^{(s)} \\ \bar{\sigma}_{xz}^{(s)} \end{vmatrix} = \begin{vmatrix} 1 & 1 & 1 & 1 \\ \alpha_1 & -\alpha_1 & -\frac{-1}{\alpha_2} & \frac{1}{\alpha_2} \\ D_1 & D_1 & D_2 & D_2 \\ D_3 & -D_3 & D_4 & -D_4 \end{vmatrix}_s \begin{vmatrix} U_1^{(s)} e^{iq\alpha_1 z} \\ 0 \\ U_3^{(s)} e^{iq\alpha_3 z} \\ 0 \end{vmatrix}_s \tag{25}$$

where the 4x4 characteristic material matrix in (25) designates the $[a_{ij}]_s$ of the substrate, and $U_1^{(s)}$ and $U_2^{(s)}$ are related to $\bar{U}_1^{(s)}$ and $\bar{U}_3^{(s)}$ in a manner similar to that of equation (24b). Notice that in equation (25) the reflected wave amplitudes $\bar{U}_2^{(s)}$ and $\bar{U}_4^{(s)}$ vanish since our solutions must be bounded for large values of $|z|$ and the substrate is considered to be an infinite half-space. Here also we α_1 and α_3 which insure boundedness at infinity. Again, z in (25) is the global coordinate.

Invoking continuity conditions (10) and using (23) and (25) with global $z = 0$, we can express the displacement and stresses at the top of layer n (i.e. the top of the plate) in terms of the substrate wave amplitudes as

$$\begin{vmatrix} u^{(n)} \\ w^{(n)} \\ \sigma^{(n)} \\ \sigma_{xz}^{(n)} \end{vmatrix}_{z=d} = \begin{vmatrix} R_{11} & R_{12} & R_{13} & R_{14} \\ R_{21} & R_{22} & R_{23} & R_{24} \\ R_{31} & R_{32} & R_{33} & R_{34} \\ R_{41} & R_{42} & R_{43} & R_{44} \end{vmatrix} \begin{vmatrix} U_1^{(s)} \\ 0 \\ U_3^{(s)} \\ 0 \end{vmatrix} \tag{26a}$$

where, from (23) and (25), we construct $[R_{ij}]$ as

$$[R_{ij}] = [A_{ij}][a_{ij}]_s \tag{26b}$$

The continuity conditions (11) can now be used to relate the wave amplitudes within the fluid with those within the substrate. Thus, invoking these conditions at the plate-fluid interface (i.e., at global z=d) and using the relations (24a) and (26a) yield

$$\begin{vmatrix} \alpha_f & -\alpha_f \\ \rho_f c^2 & \rho_f c^2 \\ 0 & 0 \end{vmatrix} \begin{vmatrix} U_1^{(f)} \\ U_2^{(f)} \end{vmatrix} = \begin{vmatrix} R_{21} & R_{23} \\ R_{31} & R_{33} \\ R_{41} & R_{43} \end{vmatrix} \begin{vmatrix} U_1^{(s)} \\ U_3^{(s)} \end{vmatrix} \tag{27}$$

Since the incident wave amplitude $\bar{U}_1^{(f)}$ is assumed to be known, the matrix equation (27) represents three equations for three unknowns. It can thus be solved to yield the reflection, longitudinal transmission, and shear transmission coefficients, respectively as

$$R = \frac{U_2^{(f)}}{U_1^{(f)}} = \frac{G_{31} - Q_f G_{21}}{G_{31} + Q_f G_{21}} \tag{28}$$

$$T_L = \frac{U_1^{(s)}}{U_1^{(f)}} = \frac{2\rho_f c^2}{G_{31} + Q_f G_{21}} \tag{29}$$

$$T_S = \frac{U_3^{(s)}}{U_1^{(f)}} = -\frac{R_{41}}{R_{43}} T_L \tag{30}$$

where

$$G_{21} = R_{21} - R_{23}\frac{R_{41}}{R_{43}}\ ,\ G_{31} = R_{31} - R_{33}\frac{R_{41}}{R_{43}}\ ,\ Q_f = \frac{\rho_f c^2}{\alpha_f} \tag{31}$$

III. SMOOTH INTERFACE CONDITION

Now, if a smooth contact interface is introduced within the plate at an arbitrary location, say the interface between layers m and m+1 then the previous analysis must be modified. In this sense, we may now consider the plate to be composed of two subplates, the top subplate with n-m layers and the bottom one with m layers, where $1 \leq m < n$. The appropriate interfacial conditions for the smooth contact surface are

$$w^{(m+1)} = w^{(m)},\ \sigma_z^{(m+1)} = \sigma_z^{(m)},\ \sigma_{xz}^{(m+1)} = \sigma_{xz}^{(m)} = 0$$

$$\text{at } z^{(m+1)} = 0\ (z^{(m)} = d^{(m)}). \tag{32}$$

First, we construct the top subplate's characteristic matrix by truncating A_{ij} starting from the top as

$$[A_{ij}]_T = [a_{ij}]_n[a_{ij}]_{n-1} \cdots [a_{ij}]_{m+1}\ . \tag{33}$$

Next, we construct the bottom subplate's characteristic matrix from the remaining part of A_{ij} as

$$[A_{ij}]_B = [a_{ij}]_m[a_{ij}]_{m-1} \cdots [a_{ij}]_1. \tag{34}$$

Hence, it is clear that $[A_{ij}] = [A_{ij}]_T[A_{ij}]_B$. Notice that when the smooth contact surface is at the plate-substrate interface (m=0) $[A_{ij}]_T$ in (33) becomes $[A_{ij}]$ and $[A_{ij}]_B$ in (34) becomes I_{4x4}. We can now write the displacements and stresses at the fluid-plate interface in terms of those at the bottom of layer m+1 by analogy with (23) and using (33)

$$\begin{vmatrix} u^{(n)} \\ w^{(n)} \\ \bar{\sigma}_z^{(n)} \\ \bar{\sigma}_{xz}^{(n)} \end{vmatrix}_{z=d} = \begin{vmatrix} A_{11} & A_{12} & A_{13} & A_{14} \\ A_{21} & A_{22} & A_{23} & A_{24} \\ A_{31} & A_{32} & A_{33} & A_{34} \\ A_{41} & A_{42} & A_{43} & A_{44} \end{vmatrix}_T \begin{vmatrix} u^{(m+1)} \\ w^{(m+1)} \\ \bar{\sigma}_z^{(m+1)} \\ \bar{\sigma}_{xz}^{(m+1)} \end{vmatrix}_{z^{(m+1)} = 0} \tag{35}$$

In the same way, we write the displacements and stresses at the top of layer m in terms of the wave amplitudes in the substrate using (34)

$$\begin{vmatrix} u^{(m)} \\ w^{(m)} \\ \bar{\sigma}_z^{(m)} \\ \bar{\sigma}_{xz}^{(m)} \end{vmatrix}_{-z_m = dm} = \begin{vmatrix} Q_{11} & Q_{12} & Q_{13} & Q_{14} \\ Q_{21} & Q_{22} & Q_{23} & Q_{24} \\ Q_{31} & Q_{32} & Q_{33} & Q_{34} \\ Q_{41} & Q_{42} & Q_{43} & Q_{44} \end{vmatrix} \begin{vmatrix} U_1^{(s)} \\ 0 \\ U_3^{(s)} \\ 0 \end{vmatrix} \tag{37a}$$

where now

$$[Q_{ij}] = [A_{ij}]_B [a_{ij}]_s. \tag{37b}$$

Invoking continuity conditions (11) and using (35) and (24a) with global z=d, we can express the displacements and stresses at the bottom of layer m+1 ($z^{m+1} = 0$) in terms of the fluid wave amplitudes as

$$\begin{vmatrix} M_{11} & M_{12} & w^{(m+1)} \\ M_{21} & M_{22} & \bar{\sigma}_z^{(m+1)} \end{vmatrix}_{z^{(m+1)}} = \begin{vmatrix} \alpha_f & -\alpha_f \\ \rho_f c^2 & \rho_f c^2 \end{vmatrix} \begin{vmatrix} U_1^{(f)} \\ U_2^{(f)} \end{vmatrix} \tag{38a}$$

where

$$M_{11} = A_{22_T} - A_{21_T} \frac{A_{42_T}}{A_{41_T}} \; ; \; M_{12} = A_{23_T} - A_{21_T} \frac{A_{43_T}}{A_{41_t}}$$

$$M_{21} = A_{32_T} - A_{31_T} \frac{A_{42_T}}{A_{41_T}} \; ; \; M_{22} = A_{33_T} - A_{31_T} \frac{A_{43_T}}{A_{41_T}}$$

and the zero shear condition at $z^{(m+1)} = 0$, from (32), has been employed.

Finally, invoking conditions (32) and using (37a) and (38a) we again obtain matrix equation (27) where now

$$\begin{vmatrix} R_{21} & R_{23} \\ R_{31} & R_{33} \\ R_{41} & R_{43} \end{vmatrix} = \begin{vmatrix} M_{11} & M_{12} & 0 \\ M_{21} & M_{22} & 0 \\ 0 & 0 & 1 \end{vmatrix} \begin{vmatrix} Q_{21} & Q_{23} \\ Q_{31} & Q_{33} \\ Q_{41} & Q_{43} \end{vmatrix} \tag{39}$$

The expressions for the reflection and transmission coefficients (28), (29), and (30) are also valid with the R_{ij} as defined in (39).

IV. QUALITATIVE DESCRIPTION OF LEAKY MODE EXTRACTION

Insight on the problem of nonspecular reflection of finite acoustic beams from fluid-solid interfaces can be gained from an examination of the reflection coefficient R as a function of angle of incidence and frequency. The expression (28) for the reflection coefficient contains, as a by-product, the characteristic equation for the propagation of modified (leaky) Rayleigh surface waves which propagate along the fluid-layered solid interface. The vanishing of the denominator in Equation (28), namely,

$$G_{31} + Q_f G_{21} = 0 \tag{40}$$

defines the characteristic equation for such waves. Furthermore, in the absence of the fluid, i.e., for $\rho_f = 0$, Eq. (40) reduces to

$$G_{31} = 0 \tag{41}$$

which defines the characteristic equation for Rayleigh surface waves on the multilayered plate bonded to a semi-infinite solid substrate.

For given real frequency ω (or fd), the real wavenumber solutions $\xi_p = k_r$ of (41) define propagating Rayleigh surface modes. It is important to indicate that in the absence of the plate only a single real solution will exist. This will be the classical surface wave mode which propagates on a

half-space. In the presence of the liquid these real wavenumbers will be perturbed rather mildly and become complex. This, of course, is confirmed by Eq. (40) which in general admits the complex solutions

$$\xi_p = k_r + i\alpha. \tag{42}$$

From Eq. (42) the phase velocity is given as $c_r = \omega/k_r$ and α is the energy leakage coefficient. Notice that α vanishes in the absence of the fluid and hence no attenuation (leaking of energy in the fluid) occurs. Hence, in the presence of the fluid these surface waves are called leaky waves. It is also known that c_r is hardly affected by the presence of the fluid [4,10-12]. However, as has been shown earlier [10-12] c_r is important because it is related to the lateral displacement of the reflected beam; in fact, the beam displacement parameter Δ_s is defined to be equal to $2/\alpha$.

Since we have concluded that the vanishing of G_{31} defines the propagating surface modes, then it is clear from (28) that as $G_{31} \to 0, R \to -1$, and we find that we have an alternative method for deducing the leaky wave propagation constant. Accordingly, the reflection coefficient at Rayleigh angle can be represented by expanding its phase factor about the incident wave vector in powers ξ and retaining the leading term [10-12]

$$R(\xi) \sim \exp[i(\xi - k_r)S'(k_r)], \tag{43}$$

where k_r is the Rayleigh wave vector, and $S'(k_r)$ is the derivative with respect to ξ of the phase of R evaluated at k_r. In refs. [10-12] we showed that

$$\Delta_s = -S'(k_r) . \tag{44}$$

Furthermore, Eqs. (43) and (42) are also valid at any incident angle above the transverse critical angle, permitting straightforward calculation of Δ_s away from the mode critical angles.

V. NUMERICAL RESULTS

For our material menu we choose steel, copper, chromium and epoxy; properties of which are collected in Table 1.

Material Type	C_L x10^5 cm/s	C_T x10^5 cm/s	ρ g/cm^3
Steel	5.69	3.13	7.9
Copper	4.76	2.32	8.9
Chromium	6.6	4.0	7.2
Epoxy	3.45	1.28	1.25

Table 1

In all of our numerical calculations we use steel for the substrate. The plate's constituents, on the other hand, can be chosen from all of the menu materials. Since it is known that chromium stiffens steel and that copper and epoxy load steel [12], we shall show that combinations of these materials (to form the plate) can either stiffen or load the steel substrate depending upon their volume fractions and ordering. Without any loss of generality the thickness d of the plate will be kept constant, and the plate's constituents (layers) will be assigned volume fractions adding to unity. Of prime importance is keeping track of the constituents order, however.

Numerical results are presented below in three different categories. In the first, we will illustrate variations of the reflection coefficient

and function G_{31} with phase velocity c (or equivalently with incident angle θ since $\sin\theta = c_f/c$). This will be done in order to display the criteria for the surface mode identification. In the second category we present dispersion relations in the form of variations of phase velocities with Fd, where F is the frequency and d is the layered plate thickness. Here comparisons of results obtained under the rigid and the smooth bondings assumptions will be displayed. Finally, in the third category we depict similar dispersion results in the forms of the variation of beam displacement Δ with Fd.

In figures 3a-3d, the variations of the real and imaginary parts of the reflection coefficients with phase velocity are shown at four values of Fd for a copper plate rigidly bonded to the steel substrate. Also displayed on this figure are normalized values of the corresponding parameters G_{31}. These figures clearly demonstrate the surface wave identification criteria where the real value of the reflection coefficient approaches -1 which also coincides with the rapid variation (through zero) of its phase and the vanishing of G_{31}. Furthermore, at Fd=0 the mode occurs at the phase velocity of 2.89×10^5 cm/s which is the surface wave speed of steel. This is expected since at the zero frequency limit, i.e., for very long wavelengths, the plate will be essentially "washed" out. As the frequency increases other modes will appear successively; this behavior is typical of all softening (loading) materials.

In figures 4a-4d, similar results are presented for a chromium plate rigidly bonded to the steel substrate. Here, the behavior is entirely different from that of figure 3a-3d except at, obviously, the zero frequency

limit. As the frequency increases, no other modes appear which is typical of stiffening materials.

Based upon the identification criteria of figures 3 and 4, we constructed in figures 5 and 6 dispersion relations curves for a copper plate attached to a steel substrate and for a chromium plate attached to a steel substrate, respectively. The solid curves correspond to rigid bonding whereas the broken curves correspond to smooth bonding to the substrate. Notice that there exists a one to one correspondence between the solid and broken curves which can be easily identified and thus compared. Notice also that the difference between corresponding solid and broken curves is most pronounced at relatively small values of Fd. For the copper plate case several modes besides the fundamental modes exist whereas for the chromium plate case only the fundamental modes exists. In both cases the phase velocity of the fundamental mode converges to the surface wave speed of the steel substrate at Fd = 0. As Fd increases the phase velocity of the copper plate case decreases to its limiting copper surface wave speed while other modes appear. The phase velocities of these higher order modes are bounded by the shear wave speeds in the steel substrate and the copper layer, respectively. This general behavior is valid for both rigid and smooth bonding; however, the slopes of corresponding solid and broken curves can vary substantially. As Fd increases from zero the phase velocity of the chromium plate increases towards the chromium's surface wave speed of 3.6×10^5 cm/sec. However, at certain values of Fd, (corresponding to a cutoff frequency) where the phase velocity reaches the steel substrate shear wave speed of 3.13×10^5 cm/s, the mode ceases to propagate. This behavior can be easily explained from the fact that, for surface waves to also exists

in the steel substrate, the phase velocity cannot exceed its shear wave speed of 3.13×10^5 cm/s. Notice also from figure 6 the dramatic contrast between the mode's behavior for the rigid and the smooth bonding situations.

In the series of figures 7-10 dispersion curves are displayed for various plates made up of equal thickness copper and chromium layers. The order of the specific plates chosen are given by c/ch, ch/c, c/ch/c/ch/c, ch/c/ch/c/ch respectively, where c stands for copper and ch for chromium. Notice, from this group of figures, the influence of layers ordering on the propagating process. The general conclusion is that for plates whose upper layer is copper the phase velocity tends to decrease at higher values of Fd and visa versa for plates with chromium top. In fact, in figure 11, we confirm this conclusion by presenting, for comparison, dispersion results obtained for a plate made up of a periodic array of 21 copper and chromium layers rigidly bonded to a steel substrate. The solid curve correspond to the case where a copper layer is at the top, and the broken curve corresponds to the change in ordering of the plate's layer, resulting in a chromium layer at the top.

In order to isolate, and quantify, the absolute influence of invoking the smooth interface condition we present in figure 12 the dispersion curves for a steel plate smoothly bonded to a steel substrate of the same material. These results are shown by the broken curves. The variation of the phase velocity should be compared with the constant value of 2.89×10^5 cm/s which correspond to the rigid bonding case, i.e., the steel plate becomes part of the steel substrate resulting in no dispersion. Also, included for comparison are results obtained for a thin epoxy plate (with volume fraction

= .01) separating the steel plate and the steel substrate. It is here assumed that the epoxy is rigidly bonded to the plate and to the substrate.

In the series of figures 13-16 we display the variations of the beam displacements as functions of Fd for the variety of multilayered plates used to generate the corresponding phase velocity dispersions of figures 7-10. Here solid curves correspond to rigid bonding whereas broken ones correspond to smooth bonding to the steel substrate. In the cases where the plate's upper layer is copper, figures 13 and 15, the phase velocity converges to that of the copper as Fd becomes large. For the case where the upper plate's layer is chromium, however, we present results up to the cut off frequency. Here the beam displacement varies from that of the steel substrate as Fd increases from zero to its cutoff value. Once again figures 12-16 show a relatively large difference between the results predicted for either rigid bonding or smooth bonding of the plate to the substrate especially at relatively low frequency ranges.

Finally, to gain further confidence in our analysis and computations we confirmed, as a special case, the numerical results reported on figure 7 of Bogy and Gracewski [15], for a two layer plate composed of nickel and silver layers rigidly bonded to a copper substrate and immersed in water.

Acknowledgement

This research has been supported by AFOSR 86-0052 grant.

References

1. A. Schoch, acoustica 2, 18 (1952).
2. W.G. Neubauer, J. Appl. Phys. 44, 48 (1973).
3. W.G. Neubauer, Physical Acoustics, edited by W.P. Mason and R.N. Thurston (Academic, New York, 1973), Vol. X, pp. 104-125.
4. H.L. Bertoni and T. Tamir, Appl. Phys. 2, 157 (1973).
5. M.A. Breazeale, L. Adler, and G.W. Scott, J. Appl. Phys. 48, 530 (1977).
6. L.E. Pitts, T.J. Plona, and W.G. Mayer, IEEE Trans. Sonics and Ultrason. SU-24, 101 (1977).
7. T.D.K. Ngoc and W.G. Mayer, J. Acoust. Soc. Am. 67, 1149 (1980).
8. D.E. Chimenti and L. Adler, Ultrasonics, 19, 112 (1981).
9. L.M. Brekhovskikh, Waves in Layered Media (Academic Press, New York, 1960) pp. 30-45.
10. A.H. Nayfeh, D.E. Chimenti, L. Adler, and R. L. Crane, J. Appl. Phys., 521, 4985 (1981).
11. D.E. Chimenti, A.H. Nayfeh and D.L. Butler, Leaky Rayleigh Waves on a Layered Halfspace. J. Appl. Phys., 53, 170-176 (1982).
12. A.H. Nayfeh and D.E. Chimenti, J. Acoust. Soc. Am. 75(5), 1860 (1985).
13. D.B. Bogy and S.M. Gracewski, J. Appl. Mech. 50, 405-414 (1983).
14. D.B. Bogy and S.M. Gracewski, J. Acoust. Soc. Am. 74, 591-599 (1983).
15. D.B. Bogy and S.M. Gracewski, Int. J. Solids Structures, 20, 8, 747-760, 1984.
16. W.T. Thomson, J. Appl. Phys. 21, 89 (1950).
17. N.A. Haskell, Bull. Seismol. Soc. Am. 43, 17-34 (1953).

18. W.M. Ewing, W.S. Jardetsky, and F. Press, Elastic Waves in Layered Media (McGraw-Hill, New York, 1957).

19. D.F. McCammon and S.T. McDaniel, J. Acoust. Soc. Am. 77, 499-507 (1985).

20. R.P. Shaw and P. Bugl, J. Acoust. Soc. Am. 46, 649-654 (1969).

21. D. Folds and C. Loggins, J. Acoust. Soc. Am. 62, 1102-1109 (1977).

22. P.D. Jackins and G.C. Gaunaurd, J. Acoust. Soc. Am. 80, 1762 (1986).

23. J. George, J. Acoust. Soc. Am. 80, 1235 (1986).

FIGURE CAPTIONS

Figure 1 The laminated plate model.

Figure 2 Representative lamina with interfacial field variables.

Figure 3 Variations of the real and imaginary parts of R and normalized values of G_{31} for a copper plate rigidly bonded to a steel half-space. Solid line = real (R), long dash = imag(R), short dash = G_{31}.

Figure 4 Variations of the real and imaginary parts of R and normalized values of G_{31} for a chromium plate rigidly bonded to a steel half-space. Solid line = real (R), long dash = imag (R), Short dash = G_{31}.

Figure 5 Dispersion relation curves for a copper plate rigidly bonded to a steel half-space (solid lines) and a copper plate in smooth contact with a steel half-space (dashed lines).

Figure 6 Dispersion relation curves for a chromium plate rigidly bonded to a steel half-space (solid lines) and a chromium plate in smooth contact with a steel half-space (dashed lined).

Figure 7 Dispersion relation curves for a plate composed of equal thickness layers of copper (top layer) and chromium in rigid contact (solid lines) with a steel half-space and in smooth contact (dashed lines) with a steel half-space.

Figure 8 Dispersion relation curves for a plate composed of equal thickness layers of chromium (top layer) and copper in rigid contact (solid line) with a steel half-space and in smooth contact (dashed line) with a steel half-space.

Figure 9 Dispersion relation curves for a plate composed of 5 equal thickness layers of copper (top) alternating with chromium in rigid contact (solid lines) and smooth contact (dashed lines) with a steel half-space.

Figure 10 Dispersion relation curves for a plate composed of 5 equal thickness layers of chromium (top) alterating with copper and in rigid contact (solid lines) and smooth contact (dashed lines) with a steel half-space.

Figure 11 Dispersion relation curves for a plate composed of a periodic array of 21 equal thickness layers of copper alternating with chromium. The solid line is for the case when the top layer is copper and the dashed line is for the case when the top layer is chromium.

Figure 12 Dispersion curves for; a steel plate in smooth contact with a steel substrate (broken curves), a steel half-space (dotted

curve), and a thin epoxy layer separating a steel plate from a substrate (solid line) with all surfaces rigidly bonded.

Figure 13 Variation of beam displacement for a plate composed of 2 equal thickness layers of copper (top) and chromium rigidly bonded (solid line) and in smooth contact (dashed line) with a steel substrate.

Figure 14 Variation of beam displacement for a plate composed of 2 equal thickness layers of chromium (top) and copper rigidly bonded (solid line) and in smooth contact (dashed line) and in smooth contact (dashed line) with a steel substrate.

Figure 15 Variation of beam displacement for a plate composed of 5 equal thickness layers of copper (top) alternating with chromium and rigidly bonded (solid line) and in smooth contact (dashed line) with a steel substrate.

Figure 16 Variation of beam displacement for a plate composed of 5 equal thickness layers of chromium (top) alternating with copper and rigidly bonded (solid line) and in smooth contact (dashed line) with a steel substrate.

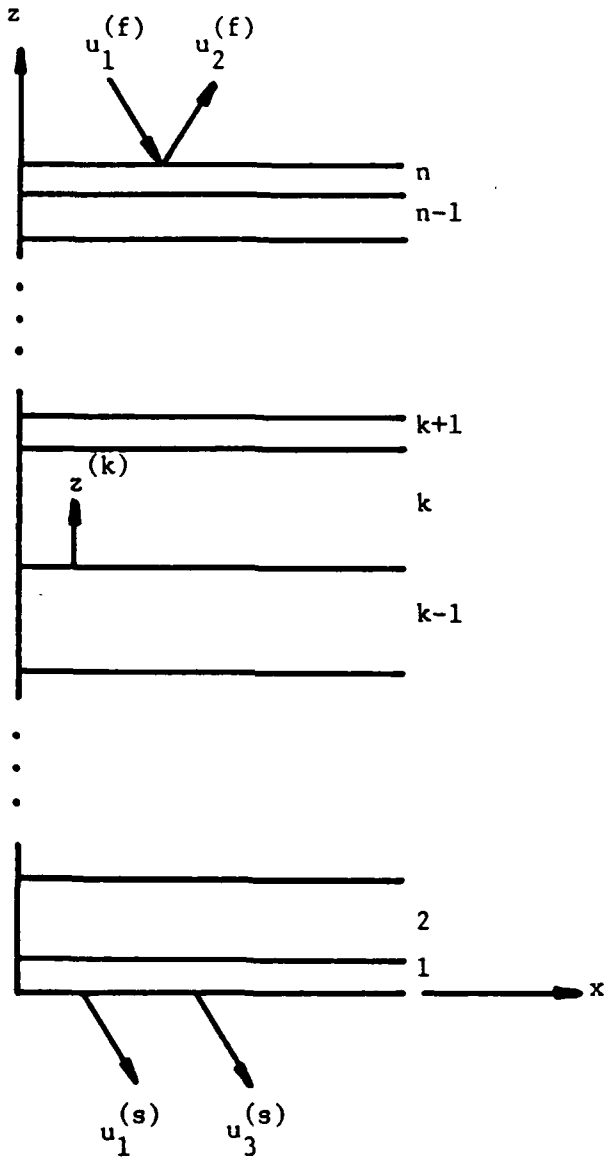

Figure 1 The laminated plate model.

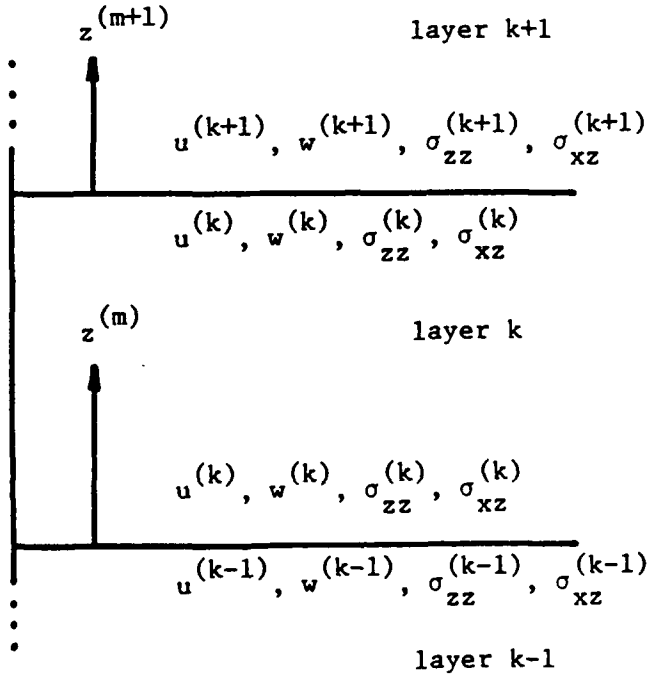

Figure 2 Representative lamina with interfacial field variables.

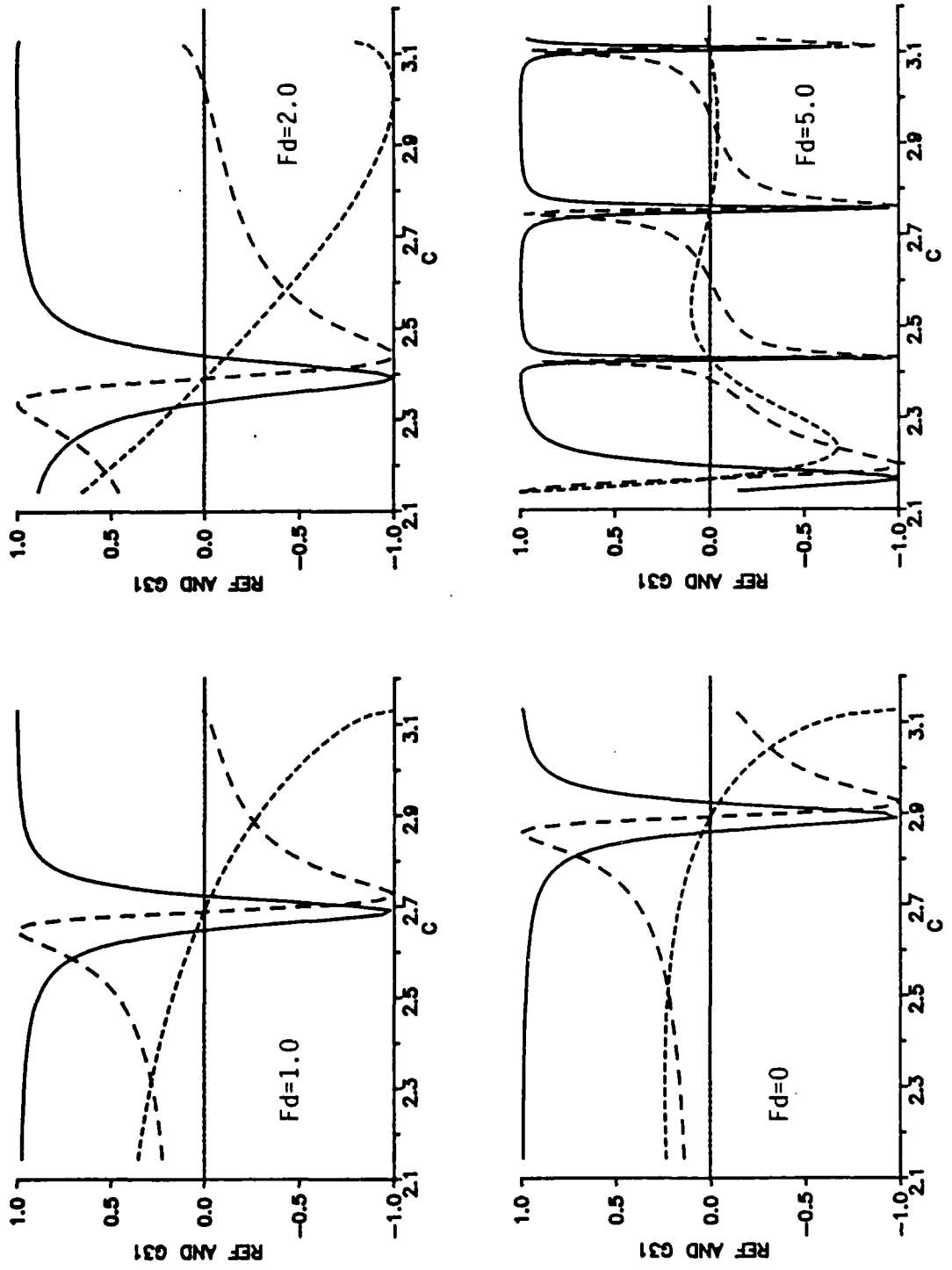

Figure 3 Variations of the real and imaginary parts of R and normalized values of G_{31} for a copper plate rigidly bonded to a steel half-space. Solid line = real (R), long dash = imag(R), short dash = G_{31}.

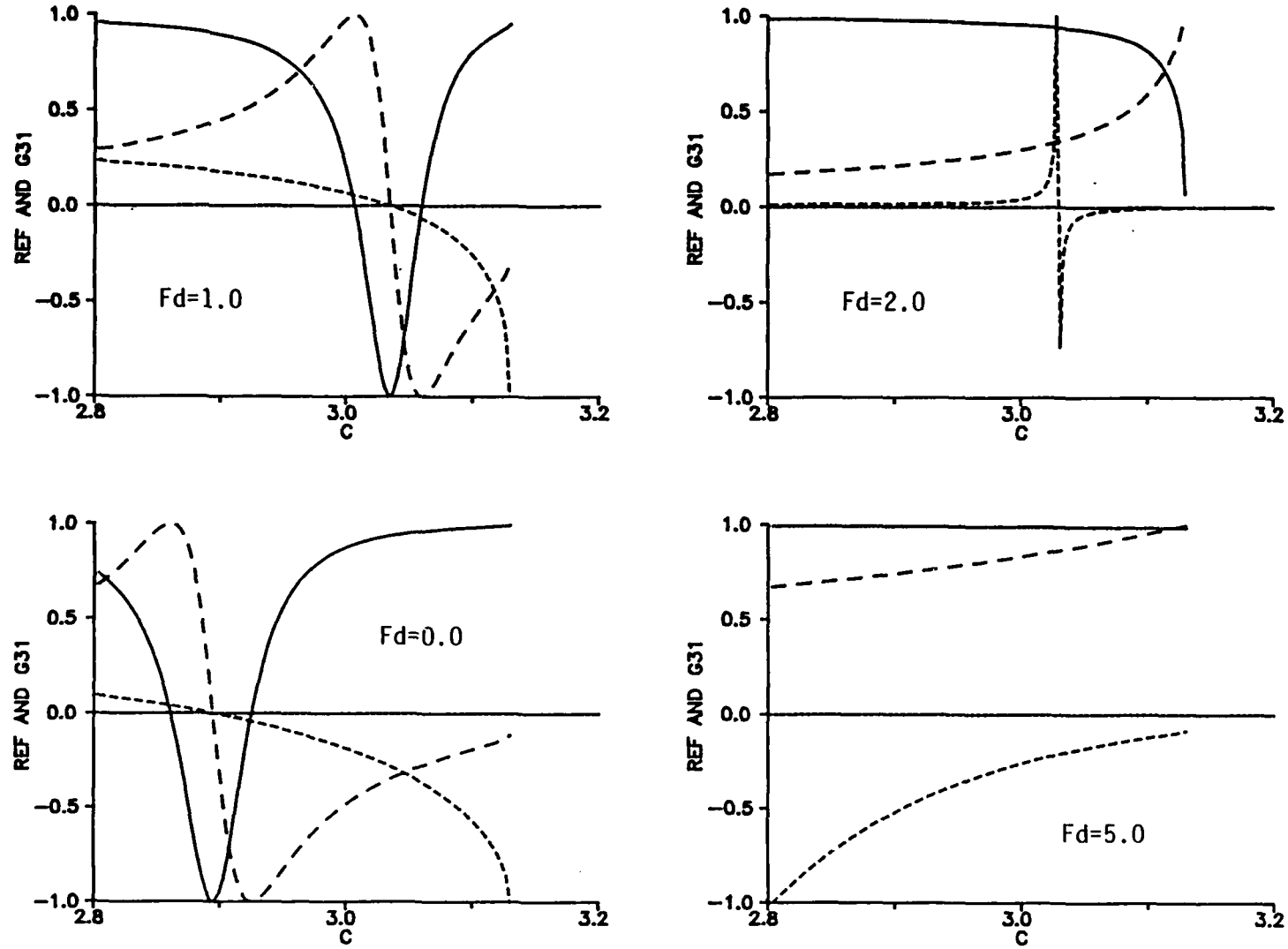

Figure 4 Variations of the real and imaginary parts of R and normalized values of G_{31} for a chromium plate rigidly bonded to a steel half-space. Solid line = real (R), long dash = imag (R), Short dash = G_{31}.

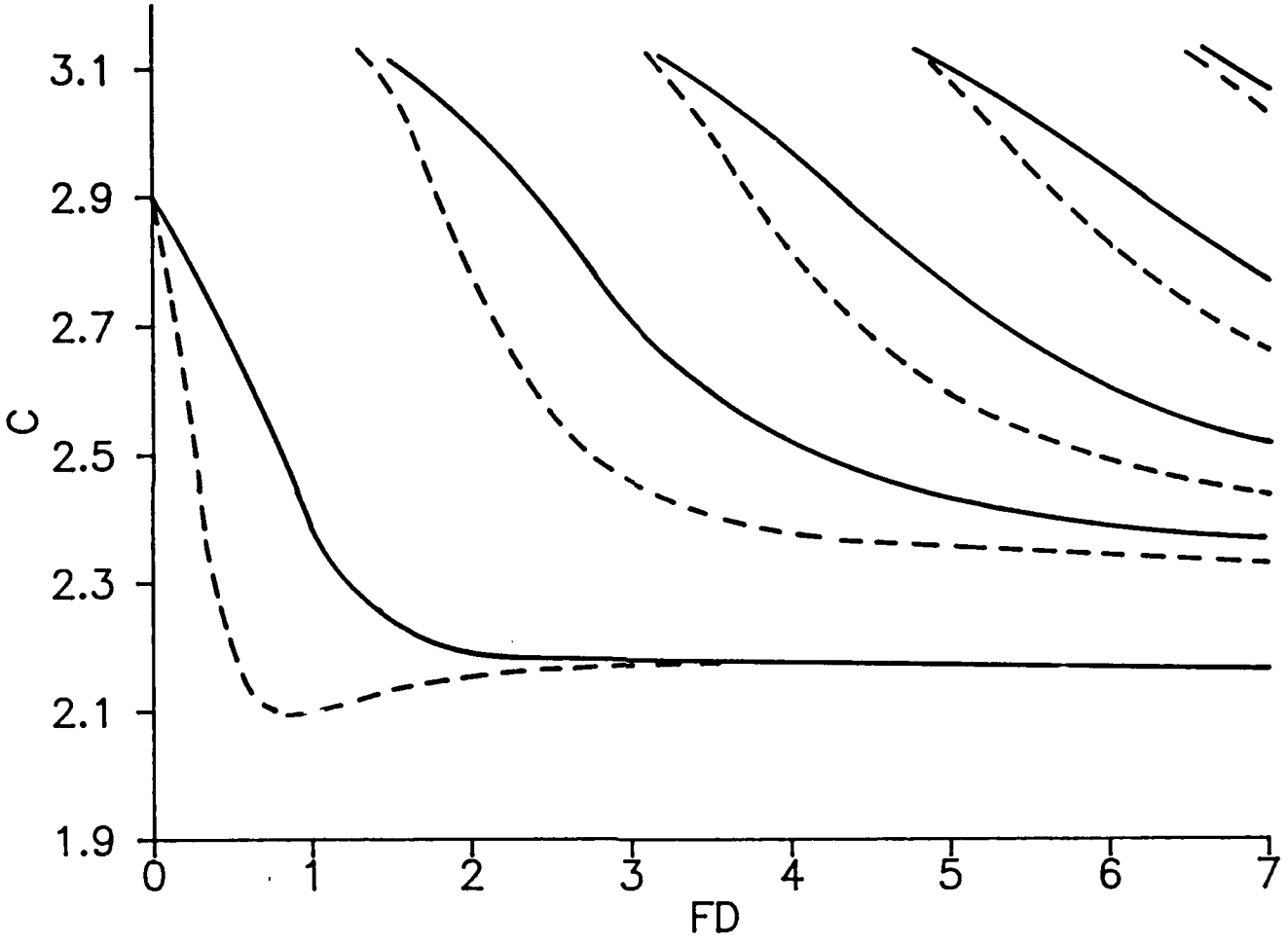

Figure 5 Dispersion relation curves for a copper plate rigidly bonded to a steel half-space (solid lines) and a copper plate in smooth contact with a steel half-space (dashed lines).

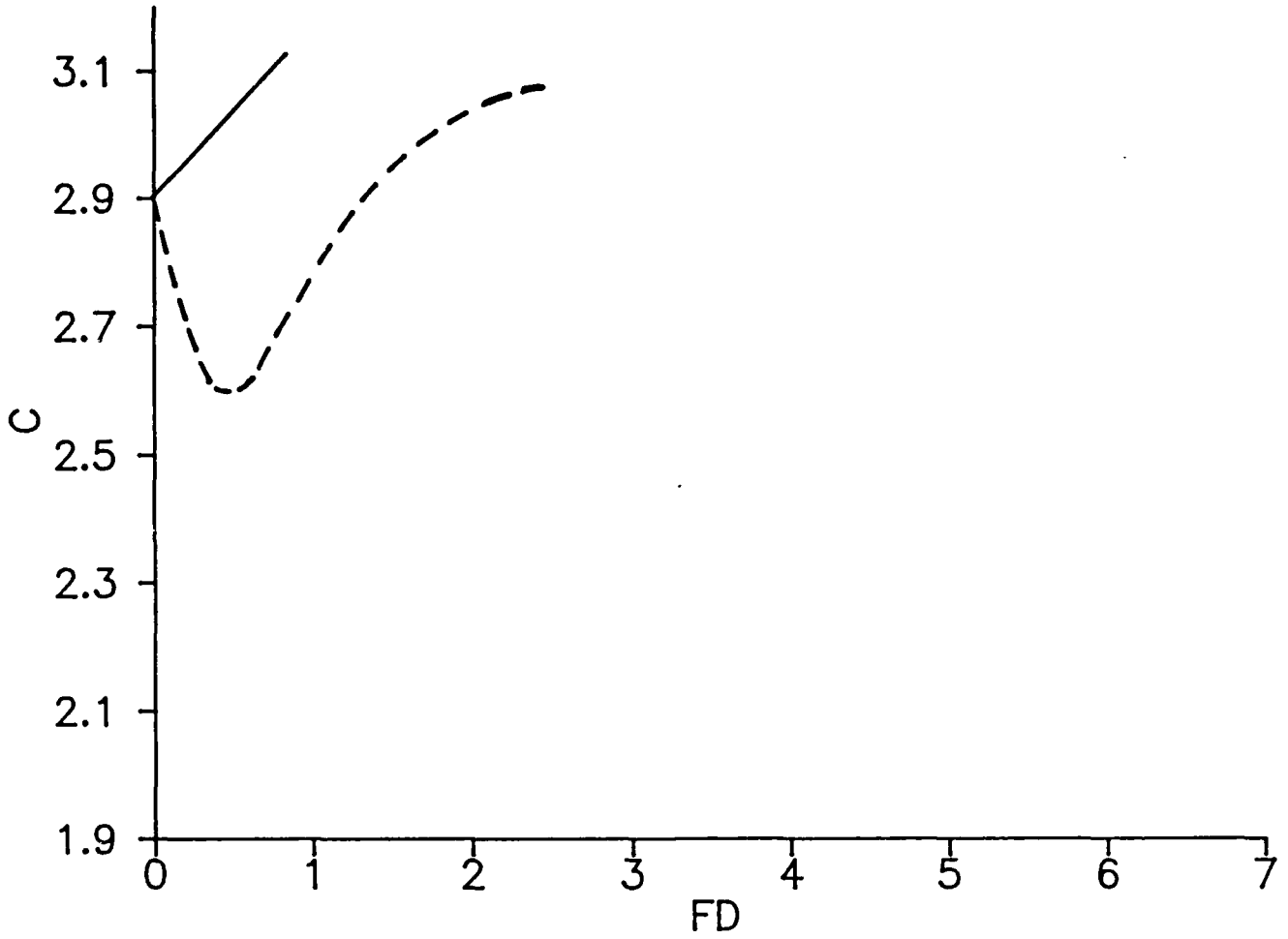

Figure 6 Dispersion relation curves for a chromium plate rigidly bonded to a steel half-space (solid lines) and a chromium plate in smooth contact with a steel half-space (dashed lined).

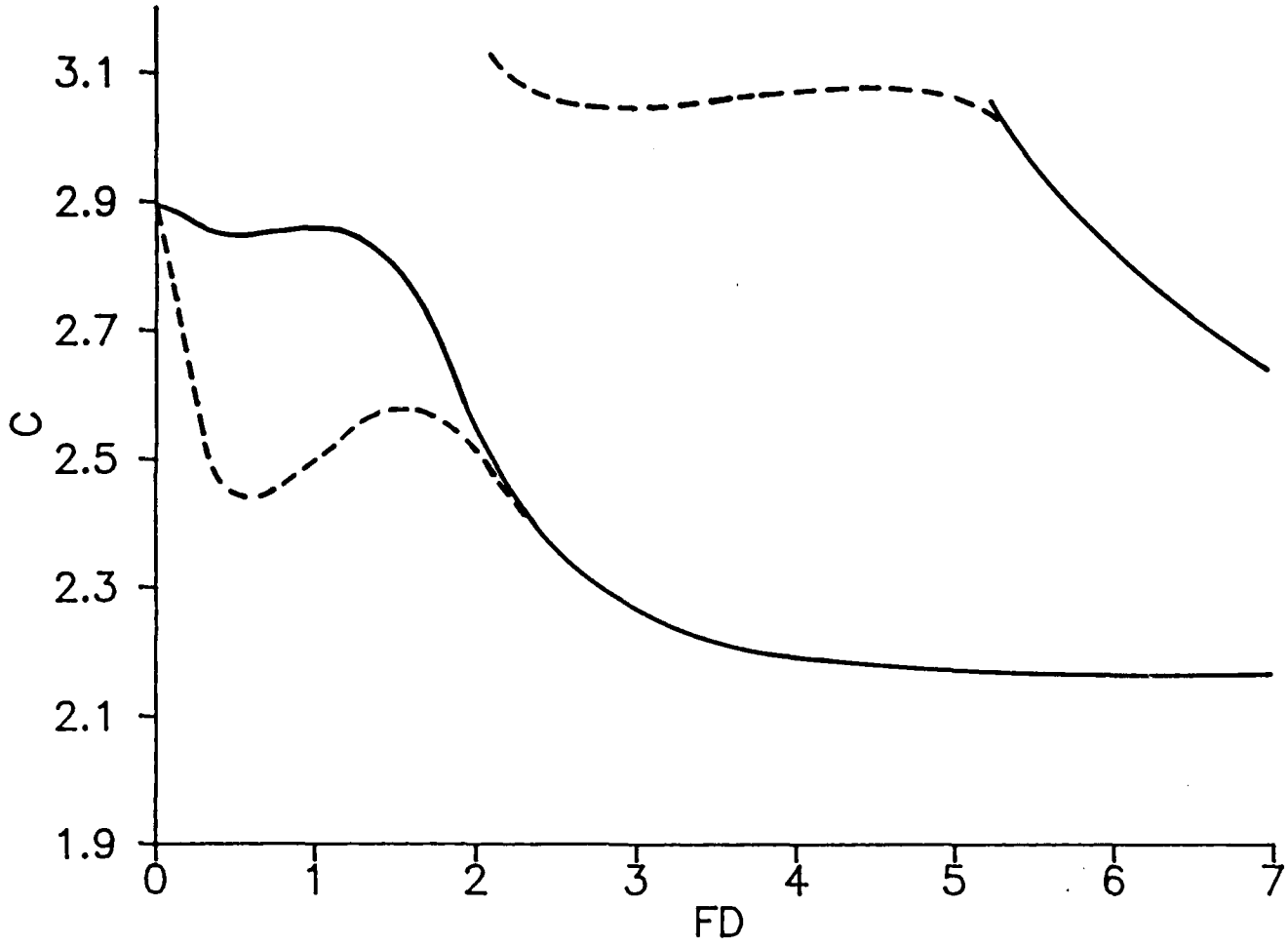

Figure 7 Dispersion relation curves for a plate composed of equal thickness layers of copper (top layer) and chromium in rigid contact (solid lines) with a steel half-space and in smooth contact (dashed lines) with a steel half-space.

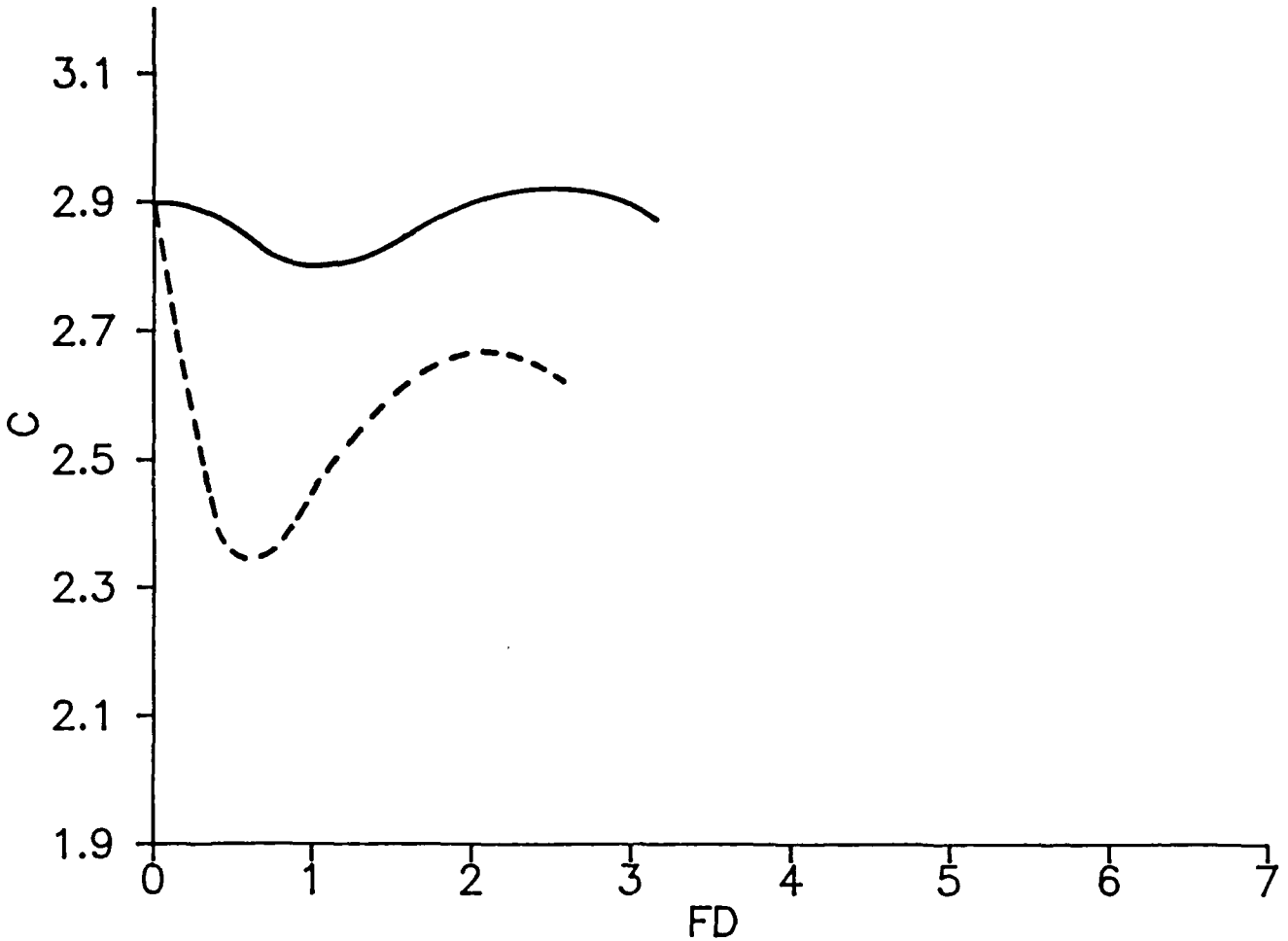

Figure 8 Dispersion relation curves for a plate composed of equal thickness layers of chromium (top layer) and copper in rigid contact (solid line) with a steel half-space and in smooth contact (dashed line) with a steel half-space.

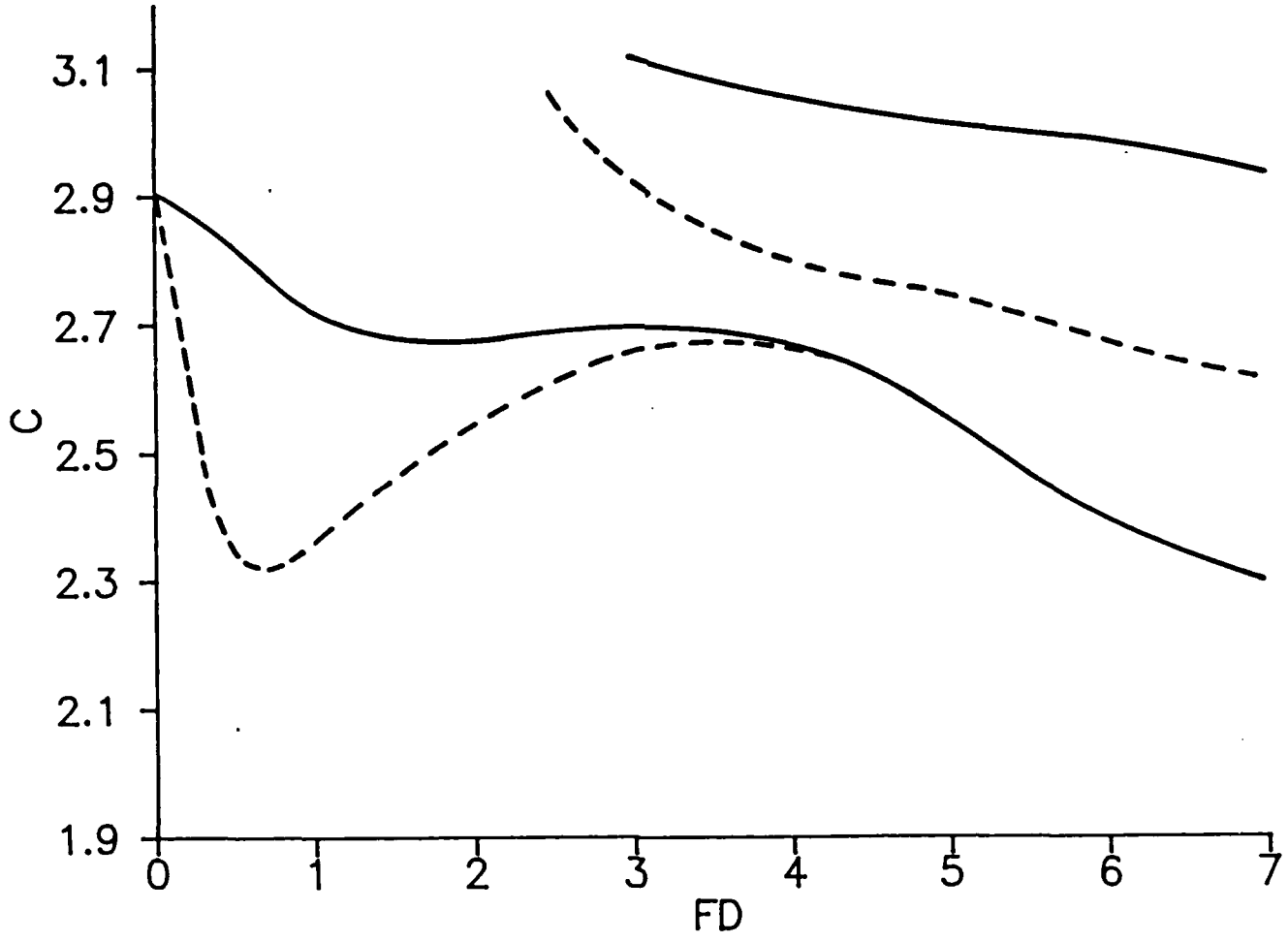

Figure 9 Dispersion relation curves for a plate composed of 5 equal thickness layers of copper (top) alternating with chromium in rigid contact (solid lines) and smooth contact (dashed lines) with a steel half-space.

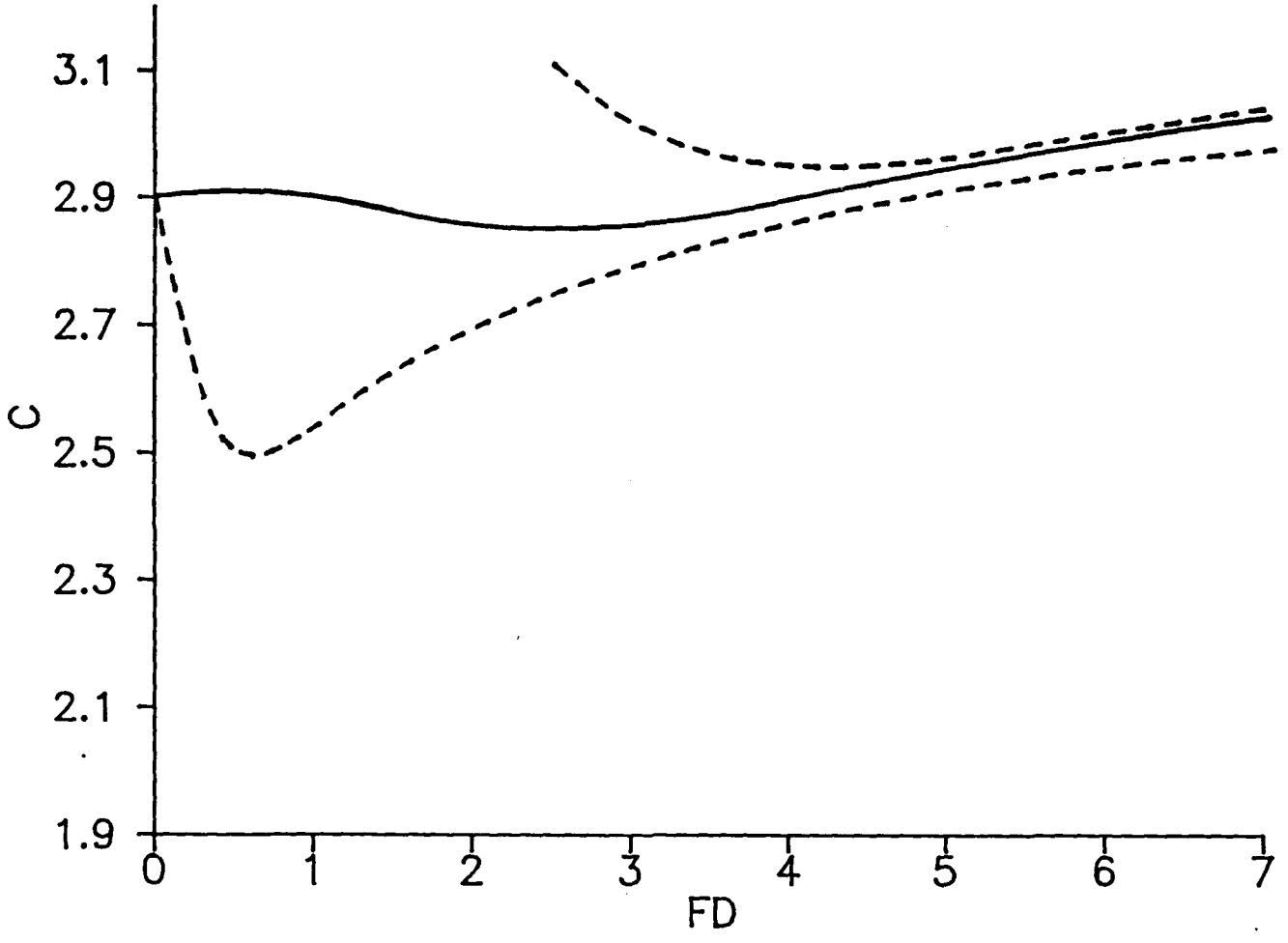

Figure 10 Dispersion relation curves for a plate composed of 5 equal thickness layers of chromium (top) alterating with copper and in rigid contact (solid lines) and smooth contact (dashed lines) with a steel half-space.

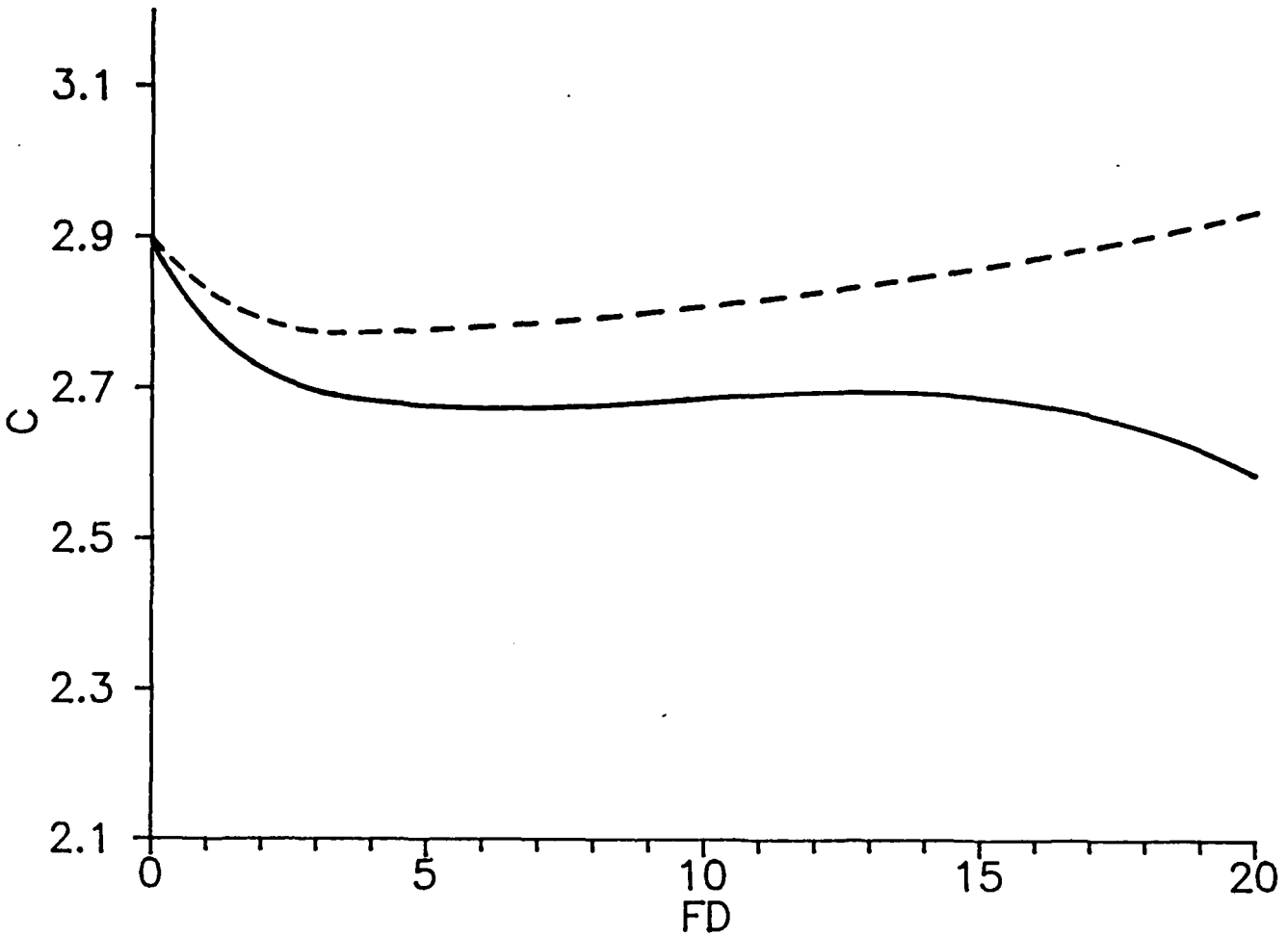

Figure 11 Dispersion relation curves for a plate composed of a periodic array of 21 equal thickness layers of copper alternating with chromium. The solid line is for the case when the top layer is copper and the dashed line is for the case when the top layer is chromium.

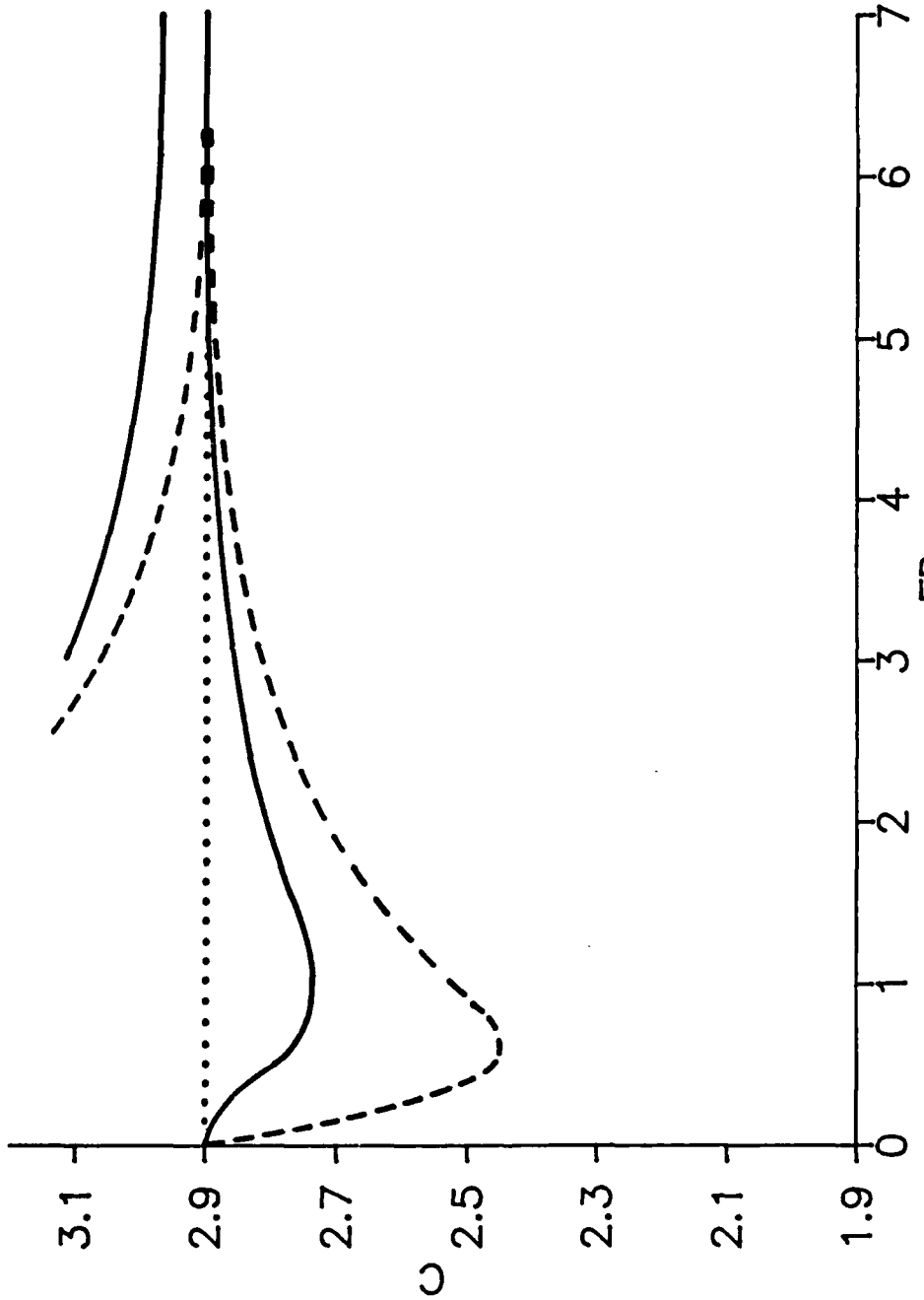

Figure 12 Dispersion curves for; a steel plate in smooth contact with a steel substrate (broken curves), a steel half-space (dotted curve), and a thin epoxy layer separating a steel plate from a substrate (solid line) with all surfaces rigidly bonded.

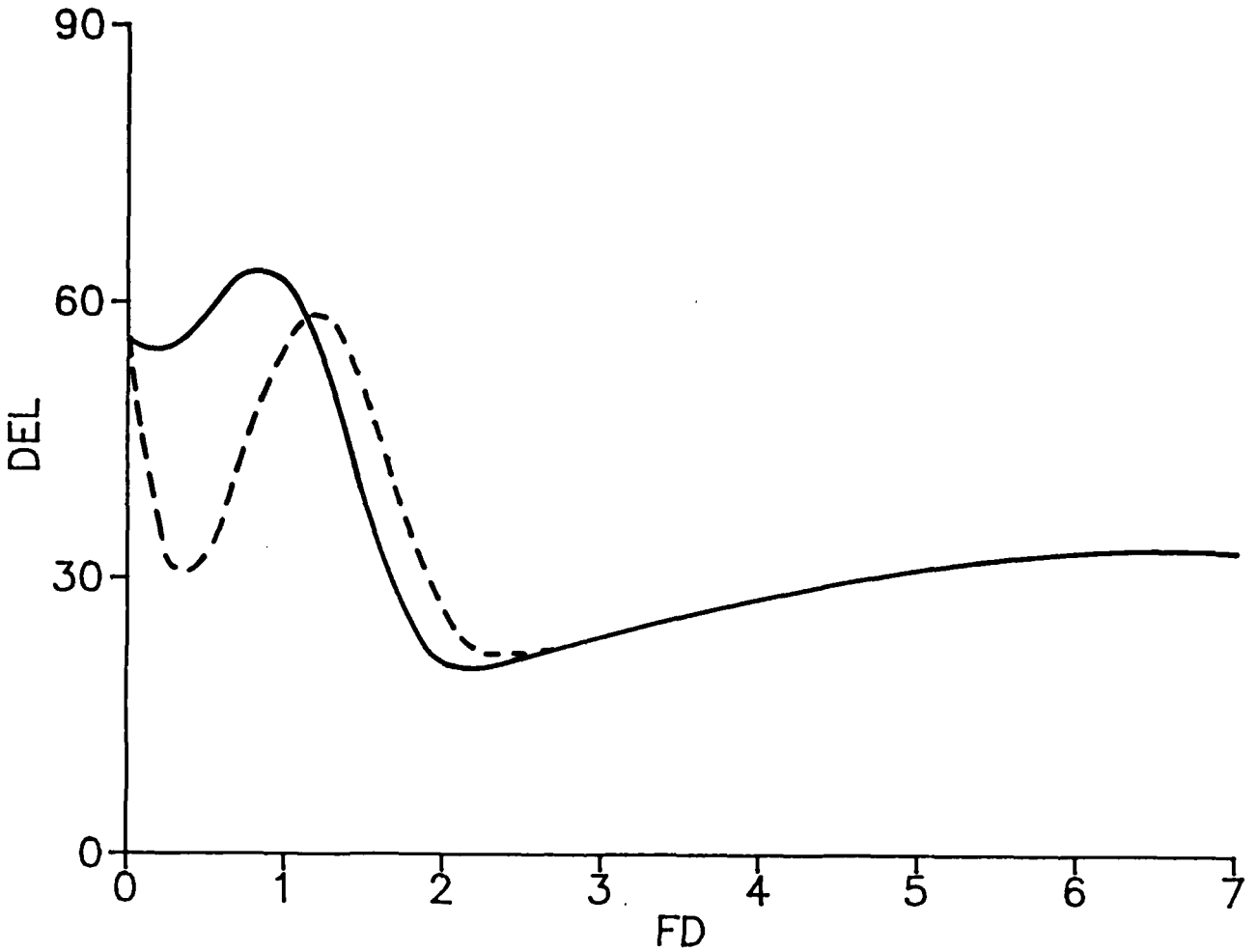

Figure 13 Variation of beam displacement for a plate composed of 2 equal thickness layers of copper (top) and chromium rigidly bonded (solid line) and in smooth contact (dashed line) with a steel substrate.

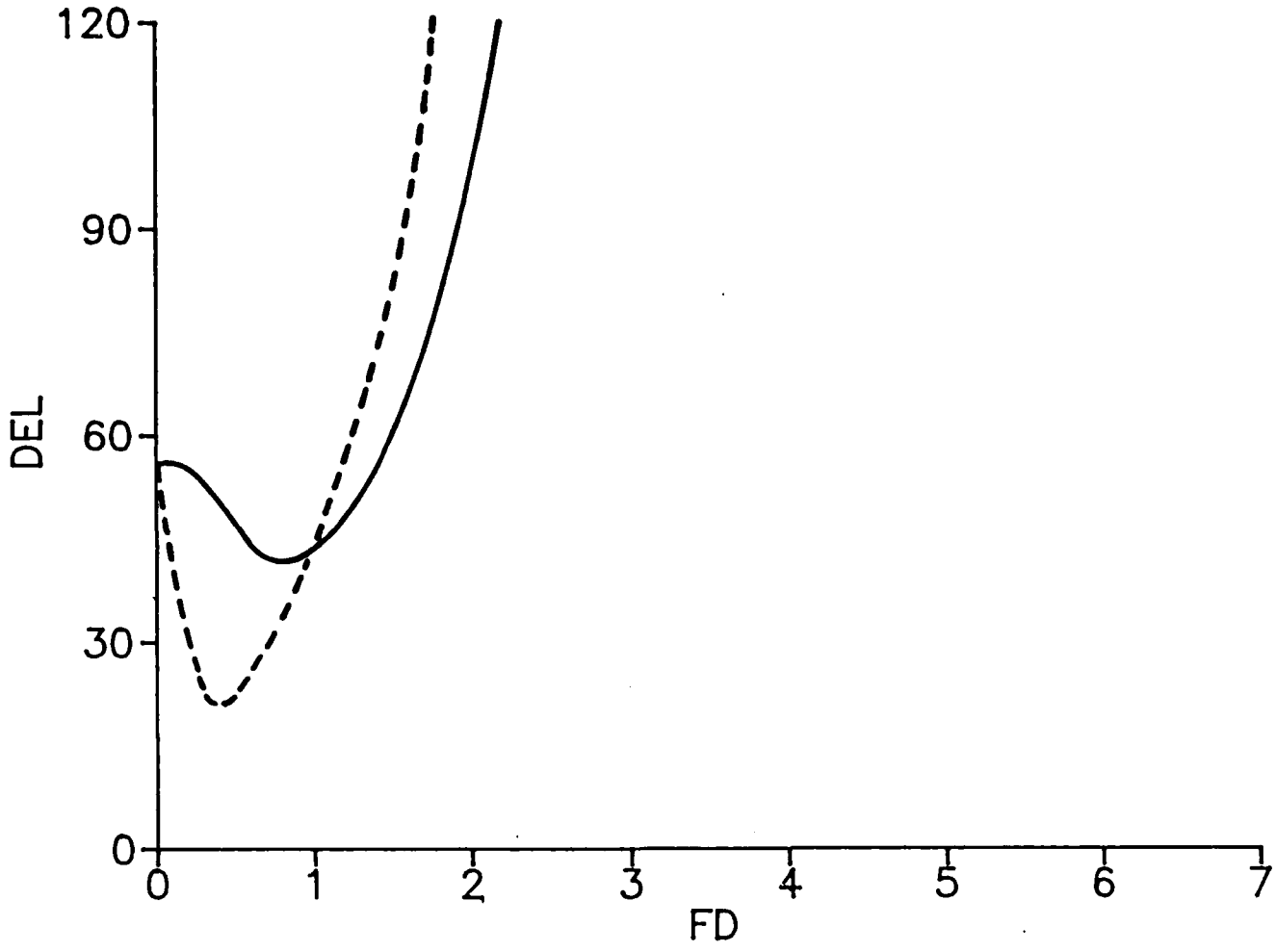

Figure 14 Variation of beam displacement for a plate composed of 2 equal thickness layers of chromium (top) and copper rigidly bonded (solid line) and in smooth contact (dashed line) and in smooth contact (dashed line) with a steel substrate.

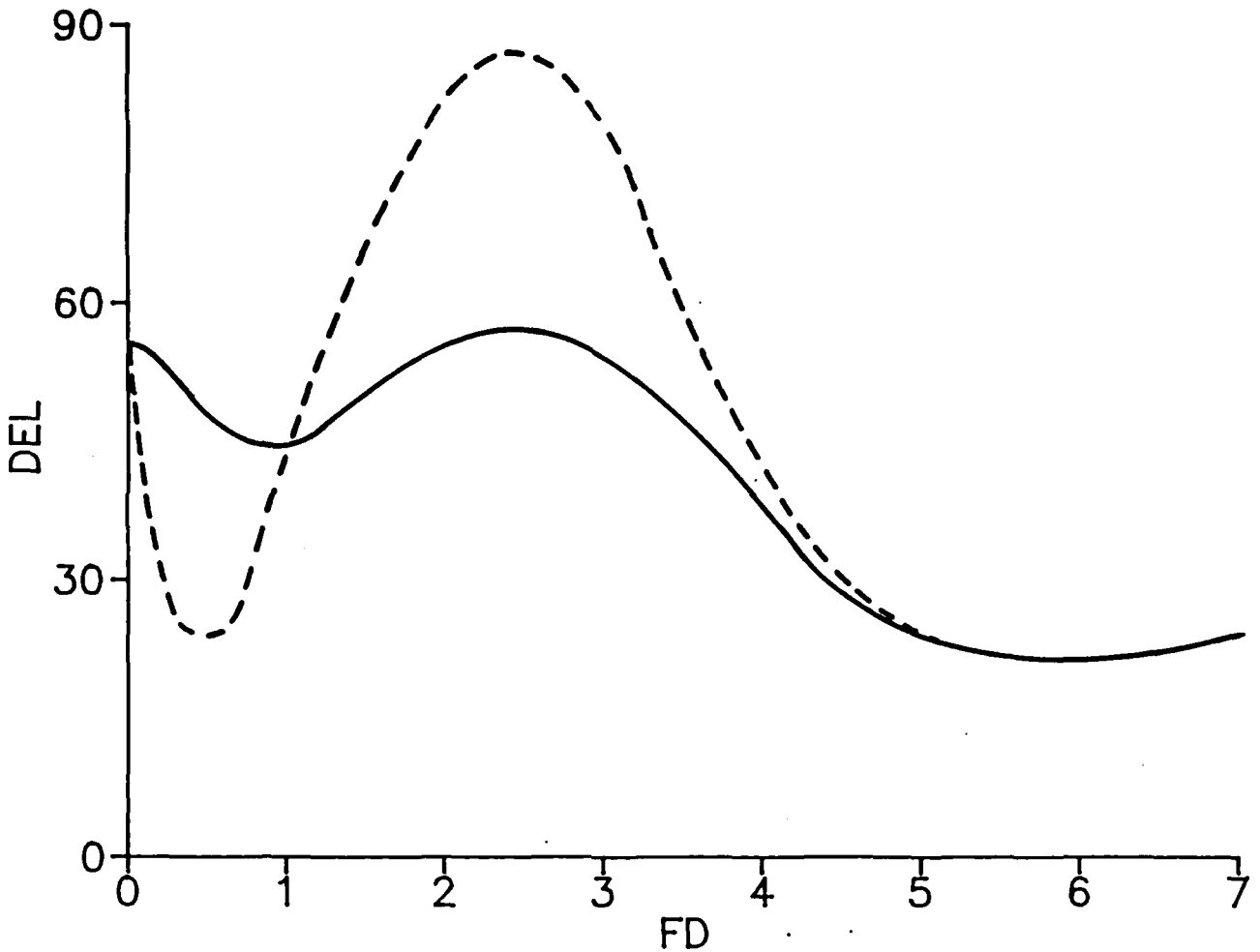

Figure 15 Variation of beam displacement for a plate composed of 5 equal thickness layers of copper (top) alternating with chromium and rigidly bonded (solid line) and in smooth contact (dashed line) with a steel substrate.

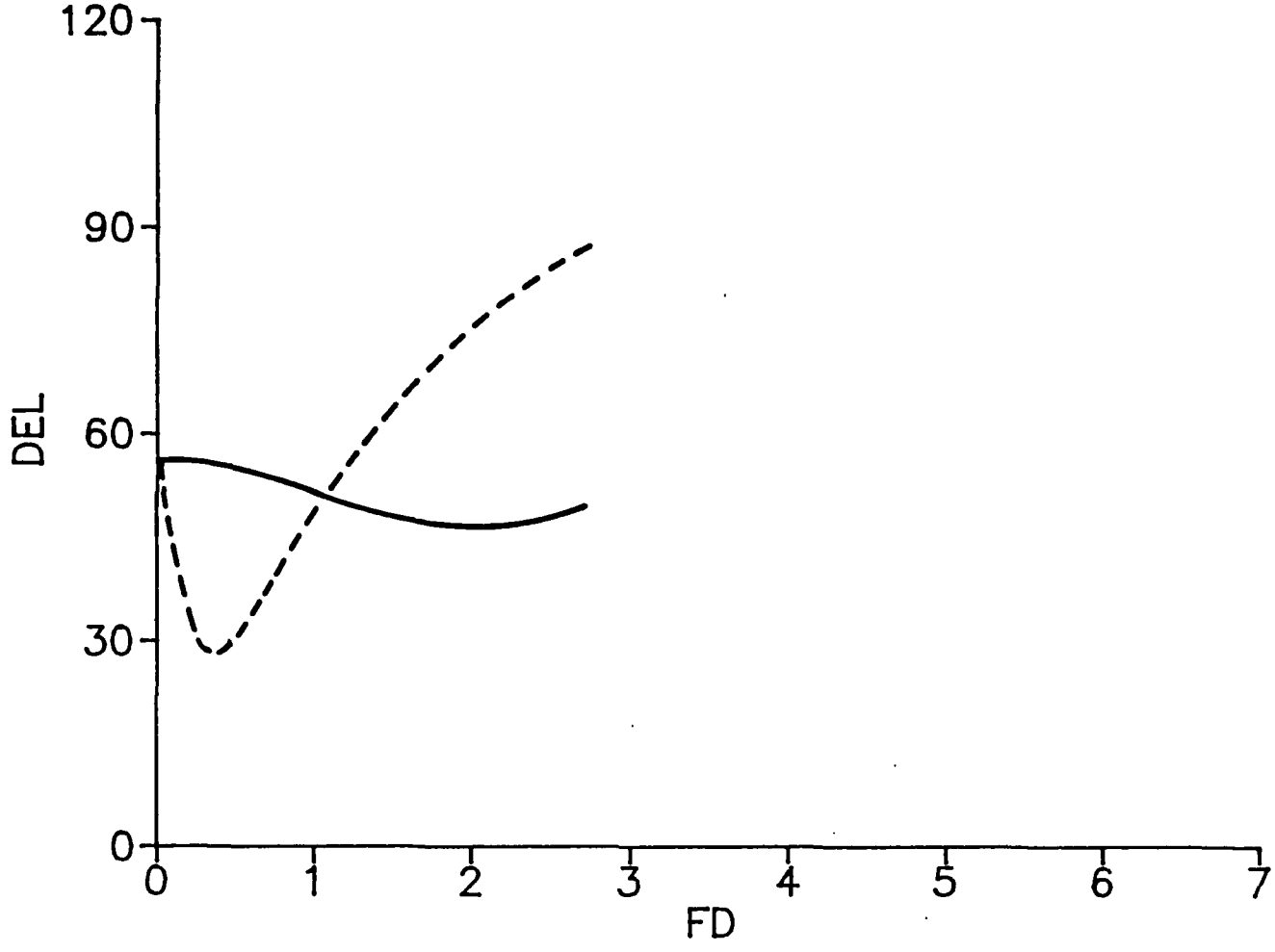

Figure 16 Variation of beam displacement for a plate composed of 5 equal thickness layers of chromium (top) alternating with copper and rigidly bonded (solid line) and in smooth contact (dashed line) with a steel substrate.

END

DATE

FILMED

5-88

DTIC